Indian Journal of Chemistry
Vol. 65, May 2026, pp. 493-519
DOI: 10.56042/ijc.v65i5.29167

Synthesis, spectral QSAR, molecular docking, DFT, ADMET studies and anti-microbial activity evaluation of some benzodioxin pyrazolines

S Balasundari[a], P Sudha[a], K Devika[b], I Muthuvel[a,c] & G Thirunarayanan*[a]

[a] Department of Chemistry, Annamalai University, Annamalainagar 608 002, Tamil Nadu, India

[b] Department of Chemistry, Thiru. Vi. Ka. Government Arts College, Thiruvarur 610 003, Tamil Nadu, India
(Affiliated to Bharathidasan University, Tiruchirappalli 620 024, Tamil Nadu, India)

[c] Department of Chemistry, M. R. Government Arts College, Mannargudi 614 001, Tamil Nadu, India
(Affiliated to Bharathidasan University, Tiruchirappalli 620 024, Tamil Nadu, India)

E-mail: drgtnarayanan@gmail.com, thirunarayanan.g.10313@annamalaiuniversity.ac.in

Received 26 February 2026; accepted (revised) 14 May 2026

A series of nine 4,5-dihydro-3-(2,3-dihydrobenzo[b][1,4]dioxin-7-yl)-1,5-(substitutedphenyl)-1*H*-pyrazolines have been synthesized by treating (*E*)-1-(2,3-dihydrobenzo[b][1,4]dioxin-6-yl)-3-phenylprop-2-en-1-ones with phenyl hydrazine hydrochloride in the presence of sodium acetate *via* cyclization reaction by cyclo-condensation process. These synthesized products have been characterized by FT-IR, ^{1}H and ^{13}C NMR spectral data. The infrared spectral frequencies C=N, N-N and C-X (ν, cm^{-1}), along with NMR chemical shifts (δ, ppm) of H_a, H_b, H_c protons, and the C=N, C-N, C-X, CH_2 carbons of 4,5-dihydro-3-(2,3-dihydrobenzo[b][1,4]dioxin-7-yl)-1,5-(substitutedphenyl)-1*H*-pyrazoline have been assigned and related to utilizing single and multi-regression analysis with Swain-Lupton's parameters and Hammett substituent constants. The *in vitro* antimicrobial assay of all compounds has been evaluated with two-gram positive bacterial species: *Staphylococcus Aureus, Streptococcus Pneumonia* and two-gram negative bacterial species: *Pseudomonas aeruginosa, Escherichia coli*, fungal species: *Candida albicans, Candida auris.* The highest values of zone of inhibition have been recorded for compound **1**, followed by the compound **4** and **8**, which exhibit good zones of inhibition both in bacterial and fungal strains. *In silico* analysis like molecular docking studies of potent antibacterial compounds (**1, 4** and **8**) indicate strong binding affinities to the receptors *Streptococcus aureus*-7S54, *Escherichia coli*-9R2Z, *Candida albicans*-5HW8. Employing DFT(B3LYP) with 6-311G(d,p) basis set for *in-silico* evaluations confirm favourable drug-likeness and pharmacokinetic properties for all pyrazolines. The ADMET properties further demonstrate that these compounds possess a good therapeutic application in combating bacterial and fungal infections.

Keywords: Pyrazolines, Hammett correlation, Anti-microbial activity**,** ADMET, pharmacokinetics

Heterocycles are extensively present in numerous natural products and are essential in metabolism due to their structural units, including vitamins, hormones, and antibiotics, as well as in pharmaceuticals, agrochemicals, and pigments[1]. Pyrazoline, is a five membered heterocyclic bio-organic compound with electron-rich bi-nitrogen present alternatively, therefore called as 1,2-diazoles and have many pharmacological effects. Because of their complex chemical properties and wide range of biological activities, these compounds have found extensive use in a variety of sectors, including materials science, medicines, agrochemicals[2,3], and insecticides[4]. Recently, the FDA has approved a lot of Several commercially accessible medications, both patented and unpatented, have prepared with pyrazole derivatives[5]. Pyrazolines are a special scaffold for the identification of small molecules used for the cure of many diseases because of their special properties, which enable them to appropriately interact with vital residues of important biological targets. Pyrazoline derivatives were reported to possess versatile biological activities such as Anti-inflammatory[6], antitumor[7], anticancer[8], anti-alzheimer's[9], antibacterial[9], antifungal[10], antidiabetic[11], antidepressant[12], analgesic[13], anti-tuberculosis[14], Anticonvulsant[15], cardiovascular[16], antioxidant[17], antihyperglycemic[18], Antiplatelet[19] and antiproliferative activity[20]. Since it can positively alter the physicochemical and biological profiles of ligands, the pyrazoline ring is also utilized as a unique bio isostere of heterocycles including imidazole, triazole, tetrazole, thiazole, oxazole, and isoxazole rings[21]. The infrared spectra of pyrazoline molecules

(1*H* pyrazoles) are used to determine how substituents will affect the vibrations (ν, cm^{-1}) of C=N, N-N and C-X. NMR spectroscopy was used to forecast the spatial arrangements of the H_a, H_b, and H_c types of protons based on their frequencies with multiplicities, such as doublet, triplet, or doublet of doublet. The effects of the substituents have been investigated and the chemical shift (δ, ppm) of the protons of the corresponding pyrazoline has been assigned based on the geometry. Sakthinathan *et al*. initially investigated the impact of substituents on 2-naphthyl based pyrazoline ring protons[22]. In their study, they assigned infrared νC=N(cm^{-1}), NMR chemical shifts for H_a, H_b, H_c, C=N (δ, ppm) values were correlated with Hammett substituent constants, F and R parameters. In these correlations they observed satisfactory r values. Such correlations not only serve in understanding reactivity and stability but also guide rational molecule design. Importantly, substituted 1H-pyrazoles have demonstrated broad-spectrum of antimicrobial activity, with several derivatives exhibiting potent antimicrobials effects against drug-resistant pathogens, where activity trends often correlate with electronic impacts predicted by Hammett relationships[22, 23]. Yang *et al*. studied the design, biological evaluation and 3D QSAR studies of novel dioxin-containing triaryl pyrazoline derivatives as potential B-Raf inhibitors[24]. Therefore, using condensation cum cyclization method[25], the authors synthesized a series of 4,5-dihydro-3-(2,3-dihydrobenzo[*b*][1,4]dioxin-7-yl)-1,5-(substitutedphenyl)-1*H*-pyrazoline derivatives with CH_3COONa catalyst, determined their structures using spectroscopy techniques. In addition to find their protein-ligand binding abilities by molecular docking study, DFT analyses, ADMET and assessed their biological activities.

Results and discussion

Chemistry

Authors taken effort to synthesized some 1*H*-pyrazoline derivatives using sodium acetate assisted condensation cum cyclization process of (*E*)-1-(2,3-dihydrobenzo[b][1,4]dioxin-6-yl)-3-phenylprop-2-en-1-ones and phenyl hydrazine in conventional method. In this condensation, more than 80% yields were obtained. Here the electron withdrawing substituents gave more yield than electron donating substituents. This condensation cum cyclization process was done using base catalyzed mechanism. The first step consists of phenyl hydrazine loses the proton and phenyl hydrazine anion formed. This anion goes to attach the carbonyl carbon of chalcone and the carbonyl oxygen gets negative charge. This oxygen negative charge was neutralized by protonation. Second step consists of loss of water by removal proton and hydroxide ions from nitrogen and carbon atoms. The third step is the loss of proton from nitrogen and this nitrogen bonded to beta carbon of chalcone. The fourth step is the rearrangement and addition of proton to beta carbons gave the pyrazolines. The plausible mechanistic route of this condensation cum cyclization was illustrated in Scheme 1.

The effect of catalyst sodium acetate on the synthesis of pyrazoline derivatives were studied for the 4,5-dihydro-3-(2,3-dihydrobenzo[b][1,4]dioxin-7-yl)-1,5-(phenyl)-1*H*-pyrazoline, (Entry **1**) by introducing the quantity of catalyst from 0.5 to 5 mg. By increasing the mentioned quantity of the catalyst, the condensation gave the product from 31 to 87 percent. The quantity of catalyst 3.5 mg of this reaction gave 87% yield. Beyond this quantity of the catalyst added, there is no improvement for the percentage of the product. This is illustrated as the statistical chart diagram in Fig. 1. From this observation the optimum quantity of the catalyst need for this condensation was found to be 3.5 mg.

Further the investigation of the optimization of catalyst of this condensation for entry **1** with the various catalyst for evaluation of the yields. In these experiments the utilized catalysts are sodium hydroxide, potassium hydroxide, barium hydroxide, zinc chloride, calcium hydroxide, sodium acetate, calcium acetate and potassium phthalate. Afore said catalysts, sodium acetate assisted condensation gave more yields (87%) than other catalysts. The optimization of catalyst of this condensation was tabulated in Table 1.

Also, the effect of solvent on the synthesis of pyrazolines were investigated with various solvents such as methanol, ethanol, acetonitrile, dichloromethane, ethyl acetate, dioxane and tetrahydrofuran. In this experiment, the ethanol medium gave more yields than other solvents. Dioxane gave lower yield of pyrazolines. The influence of solvents on the synthesis of the pyrazolines were summarized in Table 2.

Spectral correlations

The synthesised pyrazolines were characterized by their spectroscopic data such as FT-IR stretches

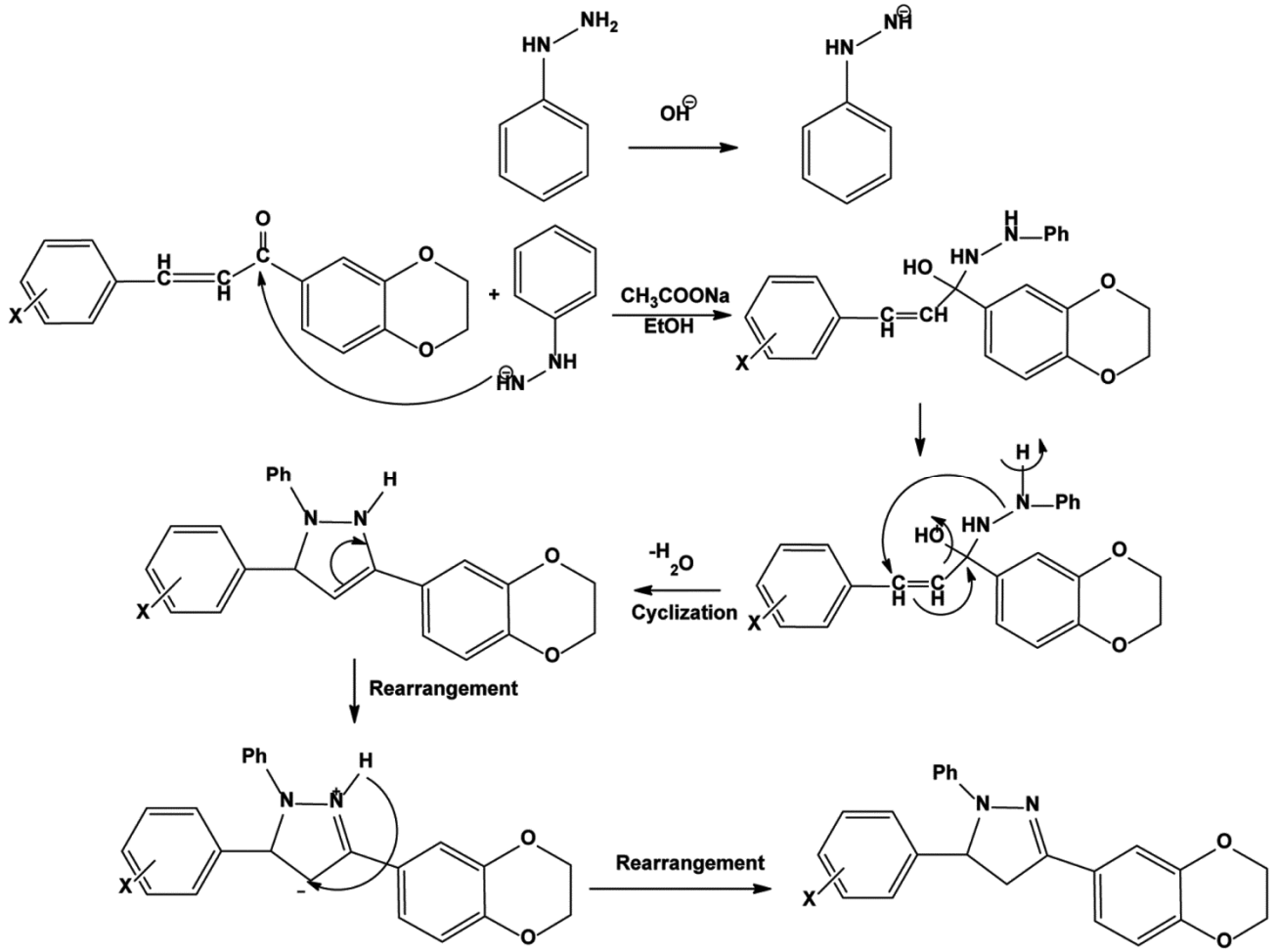

Scheme 1 — The mechanistic route for the synthesis of pyrazolines

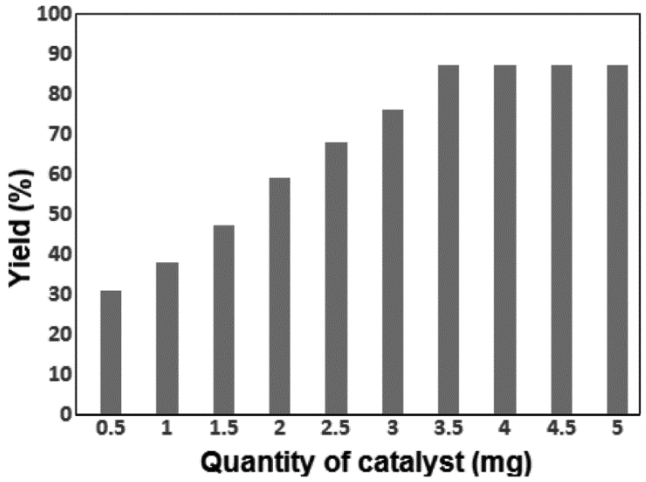

Fig. 1 — Effect of catalyst on the synthesis of pyrazoline (**1**)

Table 1 — Optimization of catalyst for the synthesis of 4,5-dihydro-3-(2,3-dihydrobenzo[b][1,4]dioxin-7-yl)-1,5-(phenyl)-1*H*-pyrazoline (Entry **1**).

Catalyst	Yield (%)
Sodium hydroxide	65
Potassium hydroxide	61
Barium hydroxide	60
Zinc chloride	58
Calcium hydroxide	63
Sodium acetate	87
Calcium acetate	43
Potassium phthalate	46

(ν, cm^{-1}) and NMR both proton and carbon-13 chemical shifts (δ, ppm). The characteristic FT-IR and NMR spectral data are illustrated in Table 3. These spectroscopical data were correlated with Hammett substituent constants and Swain-Lupton's [22, 23, 26-29, 30] parameters using single and multi-regression analysis.

Infrared spectral correlations

By analysing the substituent effects on the infrared spectral frequencies, the spectral linearity of synthesized pyrazolines has been investigated. The infrared spectral frequencies C=N, N-N and C-X

(ν, cm^{-1}) of 4,5-dihydro-3-(2,3-dihydrobenzo[b][1,4] dioxin-7-yl)-1,5-(substitutedphenyl)-1*H*-pyrazoline have been assigned in Table 3 and related to utilizing single and multi-regression analysis with Swain-Lupton's parameters and Hammett substituent constants and F and R parameters[22,23,26-29,30].

The Hammett equation utilized for the correlation analysis stating to the absorption maxima is presented in the following equation (1).

$$\nu = \rho\,\sigma + \nu_o \quad \ldots (1)$$

Table 2 — Influence of solvents on the synthesis of 4,5-dihydro-3-(2,3-dihydrobenzo[b] [1,4]dioxin-7-yl)-1,5-(substituted phenyl)-1*H*-pyrazolines

Entry	Yield (%) in the solvents						
	MeOH	EtOH	ACN	DCM	EA	DO	THF
1	74	87	66	69	59	33	49
2	80	92	59	63	46	43	55
3	83	95	68	60	48	38	52
4	74	80	49	60	45	34	54
5	70	83	58	62	65	31	53
6	69	80	53	65	56	39	50
7	79	88	58	66	53	42	58
8	84	90	68	60	55	49	62
9	79	85	62	68	55	46	56

MeOH: Methanol; EtOH: Ethanol; ACN: Acetonitrile; DCM: Dichloromethane; EA: Ethyl acetate; DO: Dioxane; THF: Tetrahydrofuran

where, ν_o is the absorption for the parent member of the series.

The assigned infrared stretches were correlated with Hammett constants and Swain-Lupton's parameters. The satisfactory correlation coefficients obtained for the infrared stretches (ν, cm^{-1}) and NMR chemical shifts (δ, ppm) from the results of statistical analyses were shown in Table 4.

From Table 4, it is evident the C=N stretching frequencies (ν, cm^{-1}) with Hammett σ_I constants, F and R parameters has shown satisfactory correlation excluding 4-OCH_3 substituent. The N-N stretching frequencies (ν, cm^{-1}) with Hammett σ_I constants and F parameters has shown satisfactory correlation. The C-X frequencies (ν, cm^{-1}) with Hammett σ, σ^+, σ_I constants and R parameters has shown satisfactory correlation excluding 4-OCH_3 substituent. The aforesaid frequencies (ν, cm^{-1}) exhibit weak correlations ($r < 0.900$) with all remaining Hammett substituent constants and F and R parameters, along with negative ρ values. This is due to the inability of the effect of substitutes on the frequencies along with restorative-conjugated structure as depicted in Fig. 2.

In view of the inability of some of the Hammett σ constants to produce individually satisfactory correlations, it was thought as valuable to pursue

Table 3 — The FT-IR stretches (ν, cm^{-1}) and NMR both proton and carbon-13 chemical shifts (δ, ppm) of 4,5-dihydro-3-(2,3-dihydrobenzo[b][1,4]dioxin-7-yl)-1,5-(substitutedphenyl)-1*H*-pyrazolines

		IR stretches (ν, cm^{-1})			^{1}H NMR chemical shifts (δ, ppm)				
Entry	X	C=N	N-N	C-X	H_a	H_b	H_c	Ar-H	X
1	H	1690	1181	–	3.08	3.78	5.22	6.73-7.32	–
2	4-Cl	1610	1136	790	3.04	3.78	5.20	6.69-7.41	–
3	4-F	1600	1120	1377	3.04	3.79	5.22	6.72-7.49	–
4	4-OH	1662	1142	3445	3.17	3.89	5.25	6.88-8.02	–
5	3-OCH_3	1668	1176	2931	3.14	4.31	5.82	6.89-8.13	2.52
6	4-OCH_3	1586	1381	2950	3.19	3.89	5.31	6.68-7.58	3.42
7	4-CH_3	1662	1287	1064	3.17	3.87	5.28	6.88-7.89	2.46
8	3-NO_2	1617	1120	1564	3.15	3.81	5.15	6.54-7.92	–
9	4-NO_2	1612	1164	1505	3.16	3.88	5.30	6.82-7.61	–

Entry	X	^{13}C NMR chemical shifts (δ, ppm)				
		C=N	C-N	C-X	Pyro-CH_2	Ar-C
1	H	146.48	64.54	126.47	43.75	113.28-145.09
2	4-Cl	146.51	64.55	133.26	43.64	113.31-144.87
3	4-F	148.07	64.69	160.89	44.70	113.31-148.07
4	4-OH	144.72	63.91	146.94	43.61	105.58-145.08
5	3-OCH_3	148.73	64.74	60.76	45.97	117.06-148.60
6	4-OCH_3	146.94	63.91	59.05	43.60	113.37-145.08
7	4-CH_3	146.91	64.21	29.74	45.11	113.37-144.96
8	3-NO_2	158.54	64.46	138.14	43.59	113.29-130.99
9	4-NO_2	158.16	64.24	146.91	45.11	113.37-144.96

Table 4 — Results of statistical analysis of infrared frequencies C=N, N-N and C-X ($\nu(cm^{-1})$), NMR chemical shifts (δ, ppm) of H_a, H_b and H_c, protons C=N, C-N, C-X and pyrazole ring CH_2 carbons of 4,5-dihydro-3-(2,3-dihydrobenzo[b][1,4]dioxin-7-yl)-1,5-(substitutedphenyl)-1*H*-pyrazolines with Hammett substituent constants (σ, σ^+, σ_I, σ_R) and F and R parameters

Freq.	Constt.	r	I	ρ	s	n	Correlated derivatives
			Infrared frequencies C=N, N-N and C-X ($\nu(cm^{-1})$)				
$\nu_{C=N}$	σ	0.741	1636.33	–33.271	35.74	9	H, 4-Cl, 4-F, 4-OH, 3-OMe, 4-OMe, 4-CH_3, 3-NO_2, 4-NO_2
	σ^+	0.742	1632.56	–15.085	37.83	9	H, 4-Cl, 4-F, 4-OH, 3-OMe, 4-OMe, 4-CH_3, 3-NO_2, 4-NO_2
	σ_I	0.947	1688.31	–99.289	28.19	8	H, 4-Cl, 4-F, 4-OH, 3-OMe, 4-CH_3, 3-NO_2, 4NO_2
	F	0.970	1670.25	–96.226	27.58	8	H, 4-Cl, 4-F, 4-OH, 3-OMe, 4-CH_3, 3-NO_2, 4-NO_2
	R	0.983	1635.20	–3.8824	39.01	9	H, 4-Cl, 4-F, 4-OH, 3-OMe, 4-OMe, 4-CH_3, 3-NO_2, 4-NO_2
ν_{N-N}	σ	0.843	1195.43	–86.489	84.69	9	H, 4-Cl, 4-F, 4-OH, 3-OMe, 4-OMe, 4-CH_3, 3-NO_2, 4-NO_2
	σ^+	0.847	1182.42	–70.495	82.53	9	H, 4-Cl, 4-F, 4-OH, 3-OMe, 4-OMe, 4-CH_3, 3-NO_2, 4-NO_2
	σ_I	0.952	1251.84	–180.519	80.16	8	H, 4-Cl, 4-F, 4-OH, 3-OMe, 4-CH_3, 3-NO_2, 4NO_2
	σ_R	0.816	1178.38	–52.880	92.66	9	H, 4-Cl, 4-F, 4-OH, 3-OMe, 4-OMe, 4-CH_3, 3-NO_2, 4-NO_2
	F	0.952	1254.31	–172.139	79.97	8	H, 4-Cl, 4-F, 4-OH, 3-OMe, 4-CH_3, 3-NO_2, 4-NO_2
	R	0.810	1175.40	–50.724	92.29	9	H, 4-Cl, 4-F, 4-OH, 3-OMe, 4-OMe, 4-CH_3, 3-NO_2, 4-NO_2
ν_{C-X}	σ	0.945	1815.16	–1184.09	82.93	7	4-Cl, 4-F, 4-OH, 3-OMe, 4-OMe, 4-CH_3, 4-NO_2
	σ^+	0.959	1618.83	–1143.4	75.58	8	4-Cl, 4-F, 4-OH, 3-OMe, 4-OMe, 4-CH_3, 3-NO_2, 4-NO_2
	σ_I	0.812	1548.02	546.386	12.48	8	4-Cl, 4-F, 4-OH, 3-OMe, 4-OMe, 4-CH_3, 3-NO_2, 4-NO_2
	σ_R	0.963	1189.51	–256.20	94.23	6	4-Cl, 4-F, 4-OH, 3-OMe, 4-OMe, 4-CH_3.
	F	0.813	1521.25	572.41	12.44	8	4-Cl, 4-F, 4-OH, 3-OMe, 4-OMe, 4-CH_3, 3-NO_2, 4-NO_2
	R	0.969	1062.47	–2396.75	87.85	8	4-Cl, 4-F, 4-OH, 3-OMe, 4-OMe, 4-CH_3, 3-NO_2, 4-NO_2
			H_a, H_b and H_c proton chemical shifts (δ, ppm)				
δH_a	σ	0.966	2.7971	1.002	0.52	8	H, 4-Cl, 4-F, 4-OH, 4-OMe, 4-CH_3, 3-NO_2, 4-NO_2
	σ^+	0.953	2.925	0.592	0.60	8	H, 4-Cl, 4-F, 4-OH, 4-OMe, 4-CH_3, 3-NO_2, 4-NO_2
	σ_I	0.932	2.575	0.837	0.67	8	H, 4-Cl, 4-F, 4-OH, 4-OMe, 4-CH_3, 3-NO_2, 4-NO_2
	σ_R	0.966	3.198	1.566	0.53	8	H, 4-Cl, 4-F, 4-OH, 4-OMe, 4-CH_3, 3-NO_2, 4-NO_2
	F	0.931	2.566	0.791	0.67	8	H, 4-Cl, 4-F, 4-OH, 4-OMe, 4-CH_3, 3-NO_2, 4-NO_2
	R	0.953	3.169	0.087	0.59	8	H, 4-Cl, 4-F, 4-OH, 4-OMe, 4-CH_3, 3-NO_2, 4-NO_2
δH_b	σ	0.948	3.789	0.391	0.33	7	H, 4-Cl, 4-F, 4-OH, 4-CH_3, 3-NO_2, 4-NO_2
	σ^+	0.930	3.833	0.181	0.36	7	H, 4-Cl, 4-F, 4-OH, 4-CH_3, 3-NO_2, 4NO_2
	σ_I	0.926	3.689	0.365	0.36	7	H, 4-Cl, 4-F, 4-OH, 4-CH_3, 3-NO_2, 4-NO_2

(*Contd.*)

Table 4 — Results of statistical analysis of infrared frequencies C=N, N-N and C-X ($\nu(cm^{-1})$), NMR chemical shifts (δ, ppm) of H_a, H_b and H_c, protons C=N, C-N, C-X and pyrazole ring CH_2 carbons of 4,5-dihydro-3-(2,3-dihydrobenzo[b][1,4]dioxin-7-yl)-1,5-(substitutedphenyl)-1*H*-pyrazolines with Hammett substituent constants (σ, σ^+, σ_I, σ_R) and F and R parameters (*Contd*.)

Freq.	Constt.	r	I	ρ	s	n	Correlated derivatives
				Infrared frequencies C=N, N-N and C-X ($\nu(cm^{-1})$			
	σ_R	0.949	3.948	0.626	0.32	8	H, 4-Cl, 4-F, 4-OH, 3-OMe, 4-OMe, 4-CH_3, 3-NO_2
	F	0.924	3.693	0.323	0.36	9	H, 4-Cl, 4-F, 4-OH, 3-OMe, 4-OMe, 4-CH_3, 3-NO_2, 4-NO_2
	R	0.936	3.692	0.387	0.35	9	H, 4-Cl, 4-F, 4-OH, 3-OMe, 4-OMe, 4-CH_3, 3-NO_2, 4-NO_2
δH_c	σ	0.965	4.878	0.846	0.46	9	*H, 4-Cl, 4-F, 4-OH, 3-OMe, 4-OMe, 4-CH_3, 3-NO_2, 4-NO_2*
	σ^+	0.962	4.996	0.599	0.47	9	H, 4-Cl, 4-F, 4-OH, 3-OMe, 4-OMe, 4-CH_3, 3-NO_2, 4-NO_2
	σ_I	0.818	4.793	0.412	0.60	9	H, 4-Cl, 4-F, 4-OH, 3-OMe, 4-OMe, 4-CH_3, 3-NO_2, 4-NO_2
	σ_R	0.969	5.237	1.418	0.43	9	H, 4-Cl, 4-F, 4-OH, 3-OMe, 4-OMe, 4-CH_3, 3-NO_2, 4-NO_2
	F	0.919	4.779	0.413	0.59	8	H, 4-Cl, 4-F, 4-OH, 3-OMe, 4-OMe, 3-NO_2, 4-NO_2
	R	0.965	5.251	1.127	0.46	9	H, 4-Cl, 4-F, 4-OH, 3-OMe, 4-OMe, 4-CH_3, 3-NO_2, 4-NO_2
				^{13}C NMR chemical shifts (δ, ppm) C=N, C-N, C-X and pyrazole ring CH_2			
$\nu_{C=N}$	σ	0.917	147.61	1.337	3.47	7	H, 4-Cl, 4-F, 4-OH, 4-OMe, 3-NO_2, 4-NO_2
	σ^+	0.936	147.91	2.034	3.27	7	H, 4-Cl, 4-F, 4-OH, 4-OMe, 3-NO_2, 4-NO_2
	σ_I	0.801	147.61	0.252	3.52	9	H, 4-Cl, 4-F, 4-OH, 3-OMe, 4-OMe, 4-CH_3, 3-NO_2, 4NO_2
	σ_R	0.916	148.12	1.994	3.47	7	H, 4-Cl, 4-OH, 3-OMe, 4-OMe, 3-NO_2, 4-NO_2
	F	0.808	147.66	0.096	3.52	9	H, 4-Cl, 4-F, 4-OH, 3-OMe, 4-OMe, 4-CH_3, 3-NO_2, 4-NO_2
	R	0.903	148.59	3.162	3.34	7	H, 4-Cl, 4-OH, 3-OMe, 4-OMe, 3-NO_2, 4-NO_2
ν_{C-X}	σ	0.924	90.63	57.586	58.04	8	H, 4-Cl, 4-F, 3-OMe, 4-OMe, 4-CH_3, 3-NO_2, 4-NO_2
	σ^+	0.926	97.25	27.079	61.71	8	H, 4-Cl, 4-F, 4-OH, 3-OMe, 4-OMe, 4-CH_3, 4-NO_2
	σ_I	0.994	27.79	193.583	36.54	9	H, 4-Cl, 4-F, 4-OH, 3-OMe, 4-OMe, 4-CH_3, 3-NO_2, 4-NO_2
	σ_R	0.804	92.50	–9.270	64.03	9	H, 4-Cl, 4-F, 4-OH, 3-OMe, 4-OMe, 4-CH_3, 3-NO_2, 4NO_2
	F	0.896	21.91	193.220	32.11	9	H, 4-Cl, 4-F, 4-OH, 3-OMe, 4-OMe, 4-CH_3, 3-NO_2, 4-NO_2
	R	0.813	87.65	–24.270	63.51	9	H, 4-Cl, 4-F, 4-OH, 3-OMe, 4-OMe, 4-CH_3, 3-NO_2, 4-NO_2
Pyro-CH_2	σ	0.825	42.959	1.088	1.98	9	H, 4-Cl, 4-F, 4-OH, 3-OMe, 4-OMe, 4-CH_3, 3-NO_2, 4-NO_2
	σ^+	0.838	43.158	1.234	1.88	9	H, 4-Cl, 4-F, 4-OH, 3-OMe, 4-OMe, 4-CH_3, 3-NO_2, 4-NO_2
	σ_I	0.842	41.94	3.168	1.85	9	H, 4-Cl, 4-F, 4-OH, 3-OMe, 4-OMe, 4-CH_3, 3-NO_2, 4-NO_2
	σ_R	0.805	42.95	–0.356	2.04	9	H, 4-Cl, 4-F, 4-OH, 3-OMe, 4-OMe, 4-CH_3, 3-NO_2, 4-NO_2
	F	0.833	42.12	2.410	1.92	9	H, 4-Cl, 4-F, 4-OH, 3-OMe, 4-OMe, 4-CH_3, 3-NO_2, 4-NO_2
	R	0.815	43.28	0.896	2.02	9	H, 4-Cl, 4-F, 4-OH, 3-OMe, 4-OMe, 4-CH_3, 3-NO_2, 4-NO_2

r=Correlation coefficient; I=intercept; ρ=slope; s=standard deviation; n=number of substituents

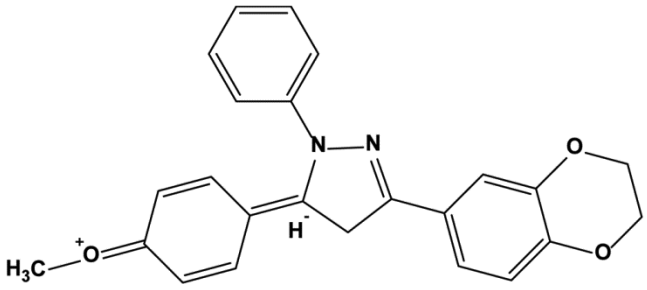

Fig. 2 — Resonance-conjugative structure

multiple correlations involving either σI and σR constants or Swain-Lupton's[30] F and R parameters. The multi-regressions gave satisfactory correlation with inductive, resonance and field effects of the substituents. This is associated with the conjugative structure shown in Fig. 2. The correlation equations for C=N, N-N and C-X are given in equations (2-7).

$\nu_{C=N}$ (cm^{-1}) = 1673.31 (±20.648) – 102.98(±42.398) σ_I +17.479 (±38.487) σ_R …(2)
(R = 0.970, n= 9, P>95%)

$\nu_{C=N}$ (cm^{-1}) = 1672.72 (±20.180) – 96.756(±39.081) σ_I +8.089 (±31.854) σ_R …(3)
(R = 0.971, n= 9, P>95%)

ν_{N-N} (cm^{-1}) = 1245.48 (±59.514) – 175.816(±122.205) σ_I – 22.234 (±110.933) σ_R …(4)
(R = 0.952, n= 9, P>95%)

ν_{N-N} (cm^{-1}) = 1241.059 (±57.733) – 169.3 (±111.807) σ_I – 43.362 (±91.129) σ_R …(5)
(R = 0.955, n= 9, P>95%)

ν_{C-X} (cm^{-1}) = 758.223(±668.042) +1130.132 (±1371.73) σ_I – 2759.68 (±1245.20) σ_R …(6)
(R = 0.967, n= 9, P>95%)

ν_{C-X} (cm^{-1}) = 778.860(±627.655) + 731.369(±1215.536) σ_I – 2428.55 (±990.733) σ_R …(7)
(R = 0.971, n= 9, P>95%)

NMR Spectral correlations

^{1}H NMR Spectral correlations

The chemical shifts (ppm) of H_a are observed at higher fields compared to those of H_b and H_c within this series of pyrazolines. This is due to deshielding of H_b and H_c which are in different chemical as well as magnetic environment. The H_a protons produced the AB pattern and the H_b proton doublet of doublet was typically well separated from the signals H_c and the aromatic protons, and the Table 3 shows the assigned chemical shifts (δ, ppm) of the protons in the pyrazoline ring H_a, H_b, and H_c. In nuclear magnetic resonance spectra, the ^{1}H or the ^{13}C chemical shifts (δ, ppm) depend on the electronic environment of the nuclei concerned. These chemical shifts have been correlated with reactivity parameters. Thus, the Hammett equation is presented in the following equation (8).

$$\text{Log } \delta = \text{Log } \delta_o + \rho\sigma \quad \ldots (8)$$

where δ_o is the ^{1}H NMR chemical shift of the corresponding parent compound.

The assigned H_a, H_b and H_c proton chemical shifts (δ, ppm) of synthesized 4,5-dihydro-3-(2,3-dihydrobenzo[b] [1,4] dioxin-7-yl)-1,5-(substituted phenyl)-1*H*-pyrazolines have been correlated with various Hammett constants. The results of statistical analysis are presented in Table 4.

From the results of Table 4, it is clear that, the H_a proton chemical shifts (δ, ppm) with Hammett σ, σ^+, σ_I, σ_R, constants, F and R parameters gave satisfactory correlation, along with positive ρ value, excluding 3-OCH_3 substituent. The resonance and field components failed in correlation. The failure in correlation is associated with the conjugative structure shown in Fig. 2. The results of statistical analysis of H_b proton chemical shifts (δ, ppm) with Hammett σ, σ^+, σ_I, σ_R, constants, F and R parameters gave satisfactory correlation, excluding 3-OCH_3, 4-OCH_3 and 4-NO_2 substituents. All correlation gave positive ρ values. The H_c proton chemical shifts (δ, ppm) with Hammett σ_I, σ, σ^+, σ_R, constant, gave satisfactory correlation, excluding 4-CH_3 substituent, along with positive ρ values. All correlations produce positive ρ values. This means that the normal substituent effect operates in all systems. The reason for failure in correlation was stated earlier, and associated with a conjugative structure, as shown in Fig. 2.

In view of the inability of some of the Hammett σ constants to produce individually satisfactory correlations, it was thought as valuable to pursue multiple correlations involving either σ_I and σ_R constants or Swain-Lupton's[30] F and R parameters. The correlation equations for H_a, H_b and H_c (δ, ppm) are given in equations (9-14).

δH_a (ppm) = 2.997(±0.382) +0.5251(±0.7862) σ_I+1.4753(±0.7137) σ_R …(9)
(R = 0.968, n= 9, P>95%)

δH_a (ppm) = 2.889 (±0.412) + 0.722(±0.798) σ_I +1.0564 (±0.6511) σ_R …(10)
(R = 0.961, n= 9, P>95%)

δH_b (ppm) = 3.856(±0.240) +0.242(±0.4936) σ_I+0.5841(±0.4480) σ_R …(11)
(R = 0.952, n= 9, P>95%)

δH_b (ppm) = 3.8079 (±0.252) + 0.2993(±0.4883) σ_I +0.3743 (±0.3980) σ_R …(12)
(R = 0.944, n= 9, P>90%)

δH_c (ppm) = 5.1933(±0.325) +0.1162(±0.668) σ_I+1.3986 (±0.6070) σ_R …(13)
(R = 0.969, n= 9, P>95%)
δH_c (ppm) = 5.1197 (±0.3334) + 0.3409(±0.6457) σ_I +1.1127 (±0.5263) σ_R …(14)
(R = 0.966, n= 9, P>95%)

^{13}C NMR Correlations

The assigned value of ^{13}C NMR chemical shifts (δ, ppm) of C=N, C-N, C-X, CH_2 carbons of 4,5-dihydro-3-(2,3-dihydrobenzo[b][1,4] dioxin-7-yl)-1,5-(substituted phenyl)-1*H*-pyrazolines are correlated with Hammett σ, σ^+, σ_I, σ_R, constants, F and R parameters[22, 23, 26-29, 30] . The results of statistical analysis were tabulated in Table 4.

From Table 4, it is observed that, the ν C=N(ppm) of 1*H* pyrazole compounds have shown satisfactory correlation with Hammett substituent constants σ, σ^+, σ_R, constants, F parameters. The remaining Hammett substituent constants σ_I and R parameters were poor correlation along with positive ρ values except 3-OCH_3, 4-CH_3, 4-F substituents. The chemical shifts δC-N (ppm) observed for the carbon of the 1*H* pyrazolines, have been correlated satisfactorily with Hammett σ, σ^+, σ_I, σ_R, constants, F and R effects of substituents were failed in single linear regression correlations with C-N chemical shifts (δ, ppm) with negative and positive ρ values. The positive and negative rho values imply that the normal and reversal substituent effect operates in all systems. The failure in correlations is the resonance and conjugative structures of the 1*H* pyrazole as shown in Fig. 2.

The chemical shifts C-X (δ, ppm) observed for the carbon of the 1*H* pyrazolines, have been correlated satisfactorily with Hammett σ, σ^+, σ_I, σ_R constants F and R parameters. The chemical shifts C-X (δ, ppm) were satisfactorily correlated with the Hammett σ, σ^+, σ_I constants. They are generally weak (r < 0.900) across all substituents. The remaining Hammett substituent constant σ_R, F and R parameters were failing in correlations. This is due to the reasons stated in earlier and associated with the resonance conjugative structure shown in Fig. 2.

The chemical shifts pyrazole ring -CH_2- (δ, ppm), have been correlated with Hammett substituent constants and F and R parameters[22, 23, 26-29, 30]. The values of all the pyrazole ring -CH_2- (δ, ppm), have shown poor correlations (r < 0.900) with all Hammett substituent constants and F and R parameters with positive ρ values, excluding 4-OH, 3-NO_2 substituents.

Since single regression analyses have shown poor correlations with few Hammett substituent constants and F & R parameters, hence it is decided to go for multi regression analysis. The multi regression analysis of chemical shift values of all pyrazolines with inductive, resonance and swain Lupton's[30] parameters produce satisfactory correlation as shown in equations (15-22)

δC=N (ppm) = 148.193(±2.589) – 0.1759(±5.316) σ_I+2.0248(±4.826) σ_R …(15)
(R = 0.916, n= 9, P>90%)

δC=N (ppm) = 148.633 (±2.4612) - 0.1110(±4.766) σ_I +3.1674 (±3.885) σ_R …(16)
(R = 0.931, n= 9, P>90%)

δC-N (δ, ppm) = 60.1673(±5.1704) – 3.5402(±10.6167) σ_I+2.0266(±9.6375) σ_R …(17)
(R = 0.916, n= 9, P>90%)

δC-N (ppm) = 61.5180 (±4.928) – 7.220(±9.5439) σ_I +1.0346 (±7.778) σ_R …(18)
(R = 0.929, n= 9, P>90%)

δC-X (ppm) = 15.018(±25.402) +203.029(±52.159) σ_I - 44.659(±47.348) σ_R …(19)
(R = 0.984, n= 9, P>95%)

δC-X (ppm) = 11.8965 (±22.041) + 195.365(±42.668) σ_I – 32.765 (±34.792) σ_R …(20)
(R = 0.980, n= 9, P>95%)

δCH_2 (ppm) = 41.6707(±1.367) +3.3682(±2.8075) σ_I – 0.9436(±2.548) σ_R …(21)
(R = 0.944, n= 9, P>90%)

δCH_2 (ppm) = 42.3695 (±1.4015) + 2.3589(±2.714) σ_I +0.7940(±2.2123) σ_R …(22)
(R = 0.936, n= 9, P>90%)

Antimicrobial potent evaluation

Antibacterial activity

The petri plates containing mm of zone of inhibitions and their statistical picture of antibacterial

activities of these pyrazolines were depicted in Fig. 3 and Fig. 4. Especially, compound **1** exhibit an excellent zone of inhibition against *S. aureus* and *E. coli*. Compound **4** and **8** exhibits a good zone of inhibition against *S. aureus*, and compound **8** exhibit an excellent zone of inhibition against *P. aeruginosa.* Compound **1** contains phenyl rings, exhibited strong

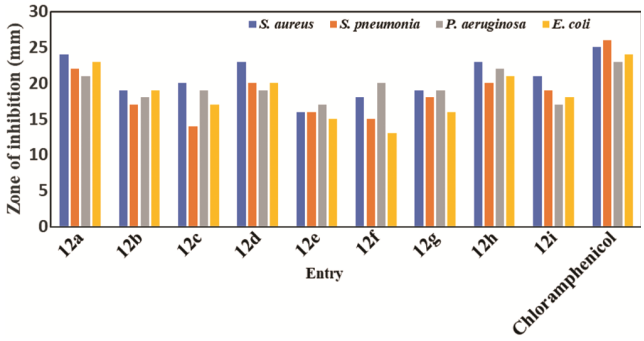

Fig. 3 — Graphical representation of antibacterial activity of synthesized pyrazolines.

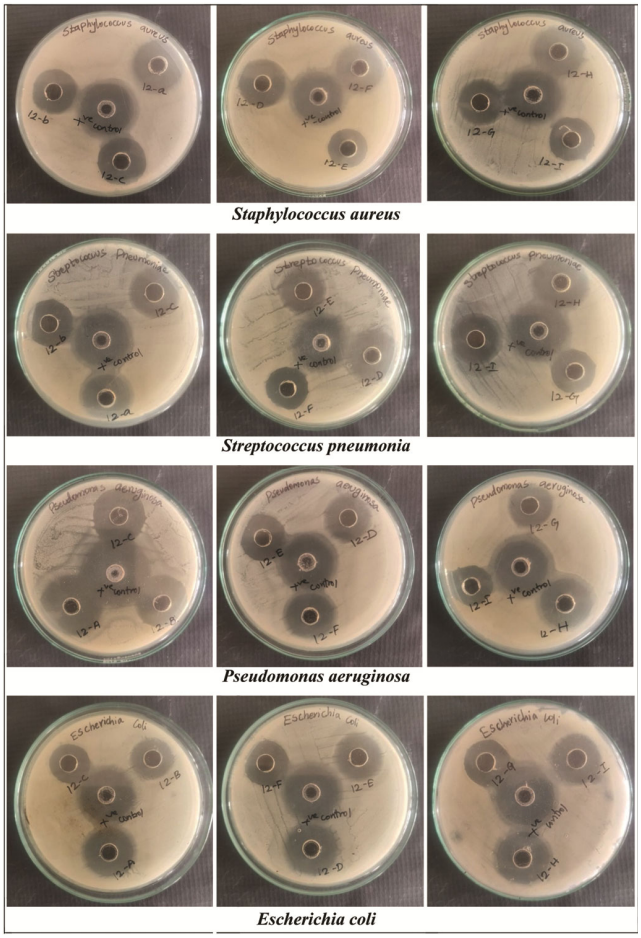

Fig. 4 — The antibacterial screening of 4,5-dihydro-3-(2,3-dihydrobenzo[b] [1,4] dioxin-7-yl)-1,5-(substituted phenyl)-1*H*-pyrazolines.

antibacterial activity against S. aureus and *E. coli*, while compounds **4** and **8** (bearing 4-hydroxy, 3-nitro substituents) demonstrated good activity. Poor activity was observed across all compounds against *S. pneumonia* likely due to the +I, +R, -I, and steric effects of the substituents. Compounds except **1, 4** and **8** exhibits moderate zone of inhibition against *E. coli*. Most of the compounds exhibited moderate to strong activity.

Antifungal efficiency

The antifungal activities of synthesized 1*H*-pyrazolines were displayed in Fig. 5 and Fig. 6 depicts the column chart and petri plates with zone of inhibition when compared with standard drug fluconazole was given in Table 5, shows that all compounds exhibited better efficiency against *C. albicans* and *C. auris.* Compound **1**, exhibits excellent zone of inhibition against *C. albicans* and *C. auris.* Compounds **1, 4, 8** and **9** (with 4-fluro, 4-hydroxy, 3-nitro and 4-nitro) shows good zone of inhibition against *C. albicans*. Compounds **1, 4** and

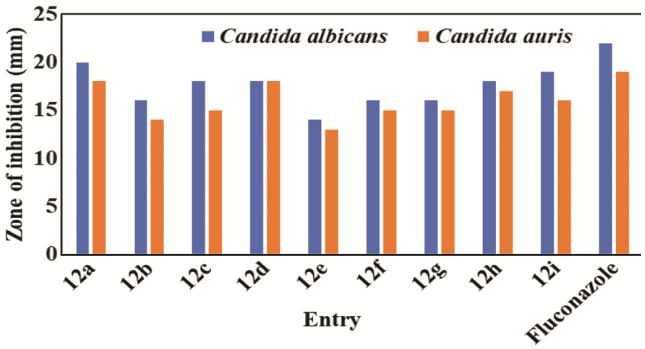

Fig. 5 — Graphical representation of antifungal activity of synthesized pyrazolines.

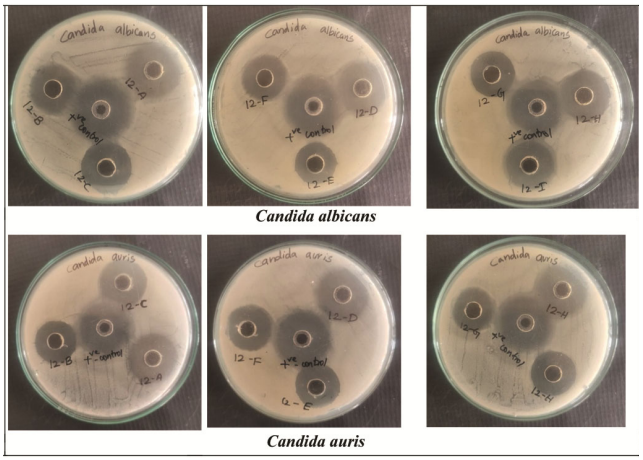

Fig. 6 — The antifungal screening of 4,5-dihydro-3-(2,3-dihydrobenzo[b] [1,4] dioxin-7-yl)-1,5-(substituted phenyl)-1*H*-pyrazolines

8 (with phenyl, 4-hydroxy and 3-nitro) shows excellent zone of inhibition against *C. auris*. The +I, +R, -I, and steric effects of phenyl, methyl, methoxy, hydroxy, and nitro groups played a crucial role in enhancing antifungal potency.

Computational analysis

Molecular Docking studies

It was noted that the standard chloramphenicol was able to bind with an affinity of –4.72 kcal/mol, while the synthesized compounds **1, 4** and **8** showed binding affinities of –7.85 kcal/mol, –7.77 kcal/mol, and –7.83 kcal/mol, respectively. In the 9R2Z *Escherichia coli* receptor the binding affinity value of standard reference chloramphenicol is –4.42 kcal/mol, while the synthesized compounds **1, 4** and **8** showed binding affinities of –6.82 kcal/mol, –6.69 kcal/mol and –6.75 kcal/mol (Table 6). The *in vitro* antifungal studies potent compounds showed that these compounds have higher affinity than *fluconazole* and improved binding affinities with the C*andida albicans* receptor 5HW8 of the target receptor compared to the fluconazole. Binding affinity of the reference standard drug fluconazole is –4.19 kcal/mol, while the synthesized compound **1, 4** and **8** showed binding affinities of –8.14 kcal/mol, –7.98 kcal/mol and –7.86 kcal/mol.

The binding conformation and molecular interaction analysis of compound **1** with the *Streptococcus aureus*- 7S54 receptor revealed that

Table 5 — The antibacterial activities of 4,5-dihydro-3-(2,3-dihydrobenzo[b] [1,4] dioxin-7-yl)-1,5-diphenyl-1*H*-pyrazolines by using two gram-positive strains and two gram-negative strains

Entry	Compound number in dish	Zone of Inhibition (mm in diameter)					
		Antibacterial activity				Antifungal activity	
		Gram-Positive		Gram-Negative		*Candida albicans*	*Candida auras*
		Staphylococcus aureus	*Streptococcus pneumonia*	*Pseudomonas aeruginosa*	*Escherichia coli*		
1	**12a**	24(15)	22(15)	21(10)	23(10)	20(15)	18(15)
2	**12b**	19(10)	17(10)	18(15)	19(15)	16(10)	14(15)
3	**12c**	20(10)	14(15)	19(10)	17(10)	18(10)	15(10)
4	**12d**	23(15)	20(15)	19(15)	20(15)	18(10)	18(15)
5	**12e**	16(10)	16(10)	17(10)	15(15)	14(10)	13(10)
6	**12f**	18(10)	15(10)	20(15)	13(10)	16(15)	15(10)
7	**12g**	19(15)	18(10)	19(10)	16(15)	16(10)	15(15)
8	**12h**	23(15)	20(15)	22(15)	21(15)	18(15)	17(10)
9	**12i**	21(10)	19(15)	17(15)	18(10)	19(10)	16(10)
Standard		Chloramphenicol				Fluconazole	
		25	26	23	24	22	19

MIC values are given in parentheses

Table 6 — Binding affinities of the investigated and reference compounds with 7S54, 9R2Z, 5HW8 receptors

Entry	Compound number	Antimicrobial stains	Binding affinity (kcal/mol)
		Streptococcus aureus-7S54	
1	**12a**		–7.85
4	**12d**		–7.77
8	**12h**		–7.83
Std.	*Chloramphenicol*)		–4.72
		Escherichia coli-9R2Z	
1	**12a**		–6.82
4	**12d**		–6.69
8	**12h**		–6.75
Std.	*Chloramphenicol*		–4.42
		Candida albicans-5HW8	
1	**12a**		–8.14
4	**12d**		–7.98
8	**12h**		–7.86
Std.	*Fluconazole*		–4.19

this compound makes multiple diverse and robust contacts with the target receptor. It was noted in the molecular contact analysis that benzodioxin group on this compound made an interaction of conventional hydrogen bonds type with ASP A:185, GLU A:194 similarly, residues ARG A: 196, TYR A: 187 linked with phenyl ring of pyrazoline. The hydroxyphenyl group linked to the pyrazoline ring of compound **4** made a conventional hydrogen bond contact with SER A: 210 residue LEU A:217, PHE A: 209 and the pyrazoline ring linked with hydrophilic amino acid SER A: 221, benzodioxin is linked with lysin moiety LYS A:148. The nitrophenyl group present in the pyrazoline ring of compound **8** is linked with TRY B:113, LYS B:87, phenyl ring attached with pyrazoline ring linked with LYS A:218, benzodioxin group on this compound made an interaction of conventional hydrogen bonds type with LYS A:223, SER A:221, VAL B:70 and residues ILE B:71, LYS A:222. Moreover, the reference standard drug *Chloramphenicol* linked with conventional hydrogen bond contact with HIS B:118, HIS B:119 and the residues VAL B: 120, PHE B: 121. Table 7 depicts the molecular conformation and contact diagrams of compounds **1, 4** and **8** and reference drug along with 7S54 receptor.

Table 7 — Binding conformation of compound **1, 4** and **8** and *Chloramphenicol* along with *Streptococcus aureus*- 7S54, *Escherichia coli*- 9R2Z and *Candida albicans*- 5HW8 receptor

Entry	*Streptococcus aureus*- 7S54	
	2D	3D
1	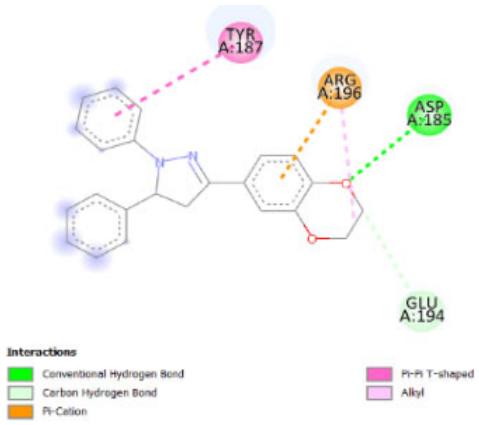	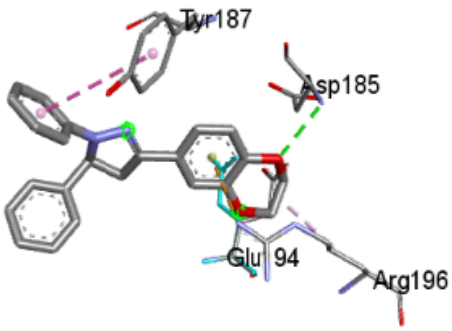
4	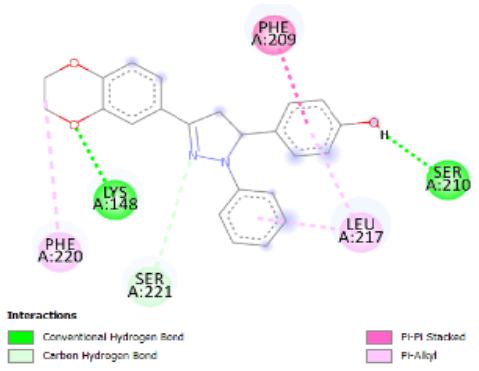	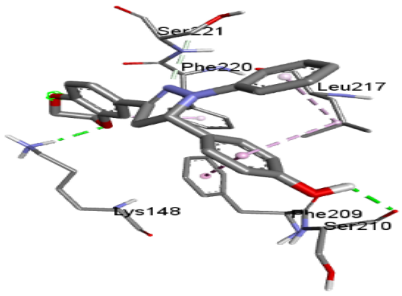
8	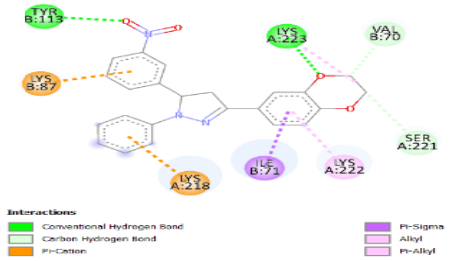	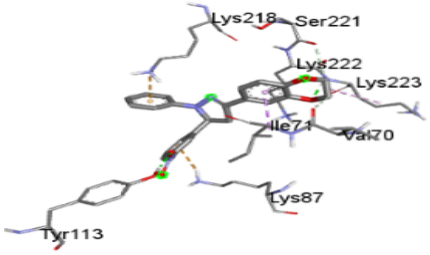

(*Contd.*)

Table 7 — Binding conformation of compound **1, 4** and **8** and *Chloramphenicol* along with *Streptococcus aureus*- 7S54, *Escherichia coli*- 9R2Z and *Candida albicans*- 5HW8 receptor (*Contd*.)

Entry	*Streptococcus aureus*- 7S54	
	2D	3D
Chloramphenicol (Ref. drug)	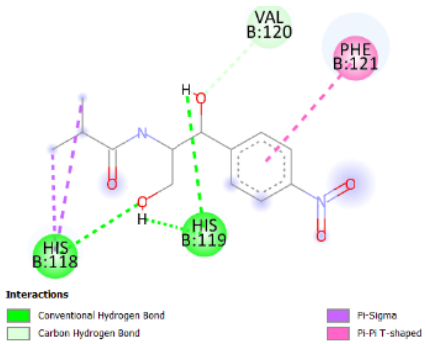	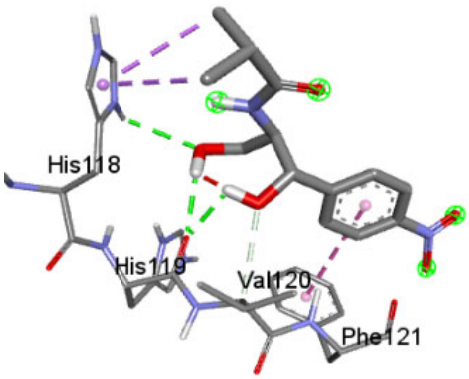
***Escherichia coli*- 9R2Z Receptor**		
1	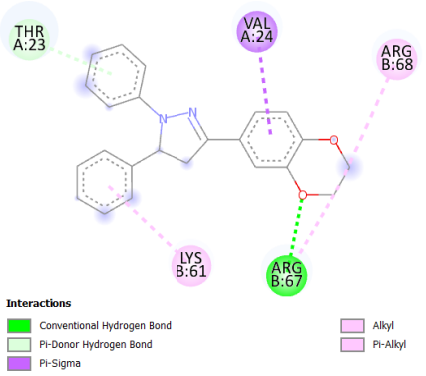	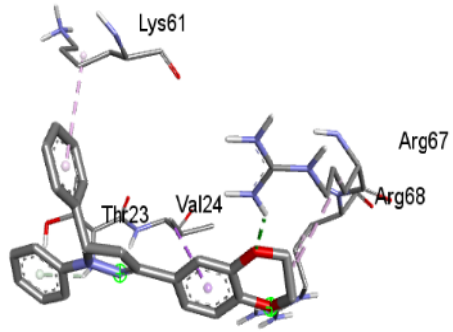
4	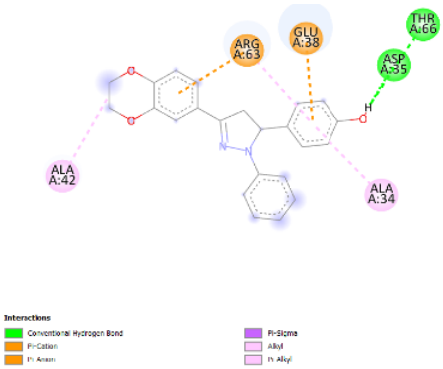	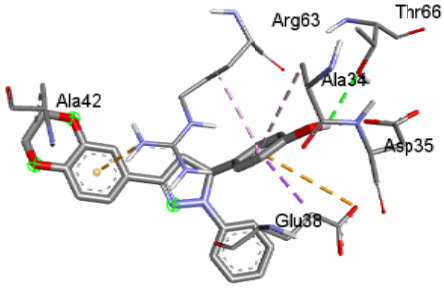
8	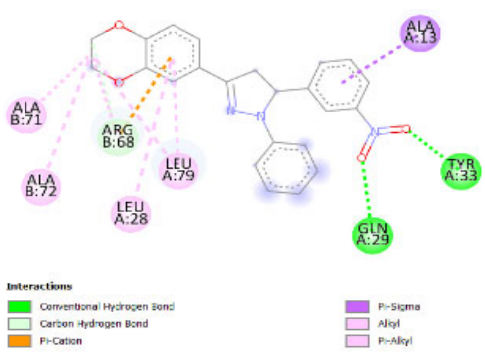	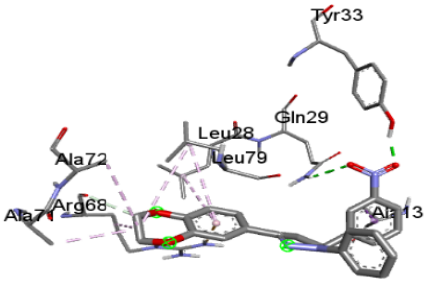

(*Contd*.)

Table 7 — Binding conformation of compound **1, 4** and **8** and *Chloramphenicol* along with *Streptococcus aureus*- 7S54, *Escherichia coli*- 9R2Z and *Candida albicans*- 5HW8 receptor (*Contd.*)

Entry	*Streptococcus aureus*- 7S54	
	2D	3D
Chloramphenicol (Ref. drug)	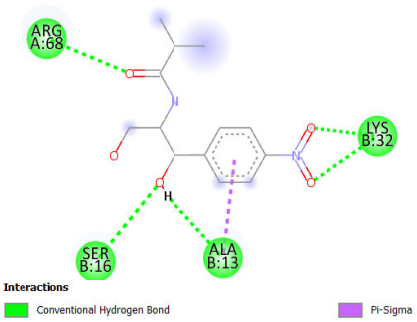	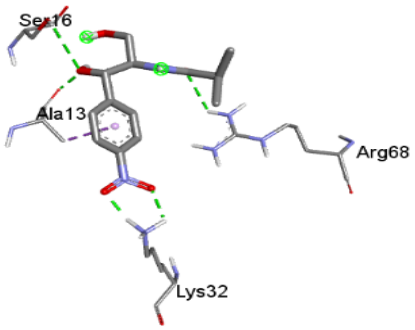
***Candida albicans*- 5HW8 Receptor**		
1	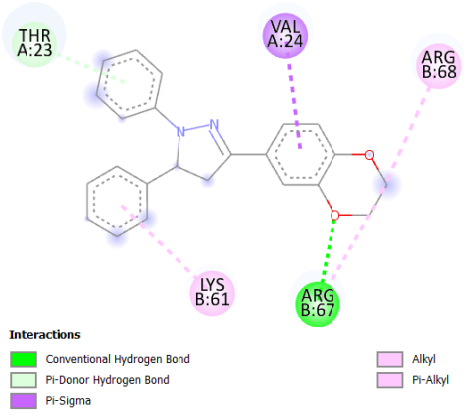	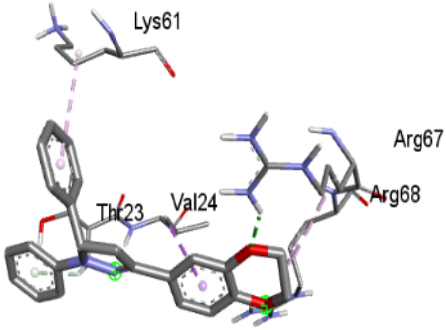
4	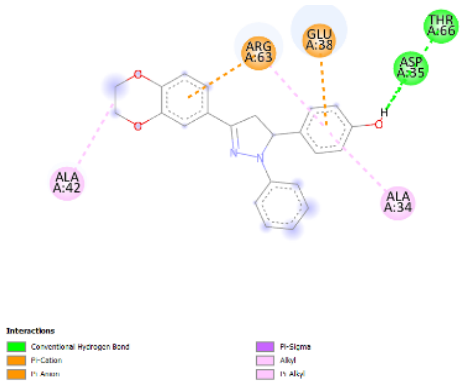	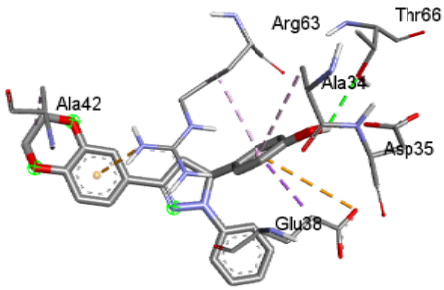
8	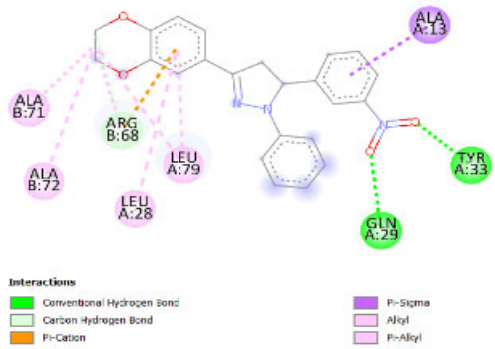	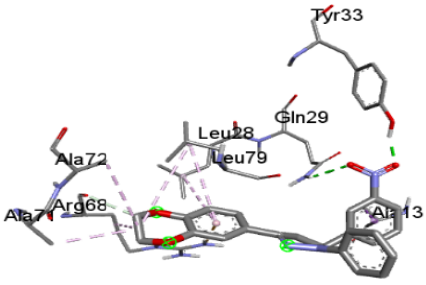

(*Contd.*)

Table 7 — Binding conformation of compound **1, 4** and **8** and *Chloramphenicol* along with *Streptococcus aureus*- 7S54, *Escherichia coli*- 9R2Z and *Candida albicans*- 5HW8 receptor (*Contd*.)

Entry	*Streptococcus aureus*- 7S54	
	2D	3D
'\Chloramphenicol (Ref. drug)	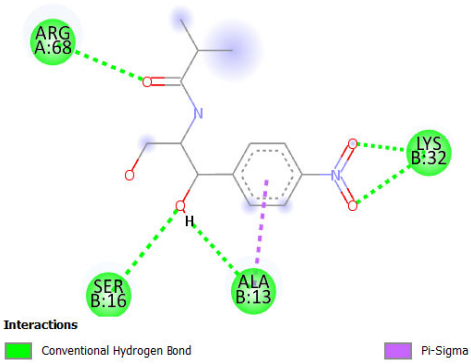	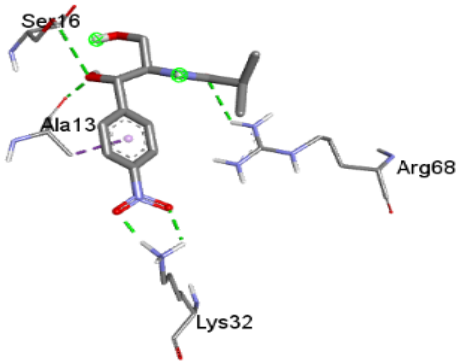

The binding conformation and molecular interaction analysis of compound **1** with the *Escherichia coli*- 9R2Z Receptor revealed that this compound's benzodioxin group attached with pyrazoline ring of compound linked with arginine moiety ARG B: 67 of conventional hydrogen bond, this compound also contributed multiple hydrophobic contacts, and electrostatic contacts (Pi-Sigma, Alkyl, and PiAlkyl type) interaction with ARG B: 68, VAL A: 24, LYS B: 61. The hydroxyphenyl group linked to the pyrazoline ring of this compound **4** also contributed multiple conventional hydrogen bond, ASP A:35, THR A:66, multiple hydrophobic contacts, and electrostatic contacts (Pi-Sigma, Alkyl, and PiAlkyl type) interaction with both the adjacent groups of pyrazoline moiety, ALA A:34, ALA A:42. Table 7 shows the binding conformation of compounds and reference drug along with 9R2Z Receptor. The nitrophenyl group present in the pyrazoline ring of compound **8** is linked with GLN A:29, TRY A:33and residues ALA A:30, the benzodioxin group linked with multiple hydrophobic contacts, and electrostatic interaction with ALA B:71, ALA B:72, LEU A: 28, LEU A:28 and ARG B:68. The reference drug linked with multiple conventional hydrogen bonds such as ALA B:13, ARG A:68, LYS B:32, SER B: 16 with the anti-fungal receptor.

The binding conformation and molecular interaction analysis of *in vitro* potent compounds with the *Candida albicans*- 5HW8 Receptor. The data in Table 7 shows that compound **1** exhibited the best binding efficiency against the fungal receptor, Dioxin that links with GLY F:104, nitrogen of pyrazoline ring links with GLN E:58 as conventional hydrogen bond and residues as ILE F:106 and LEU F:34, PRO B:130, PRO F:108. The *in-silico* studies highlighted the importance of hydrogen bond interactions of compound **4**, hydroxy links with alpha-amino acid GLU B:39, dioxin links with LYS E:45 residues such as LYS B:38, GLY E:47, ARG E:44, ARG E:46. In the compound **8,** nitrophenyl ring of pyrazoline links with GLU F;3, LYS C:80 as conventional hydrogen bond and residues GLY C:75, ASN F:70, TYR F:71, LEU C:78, PRO C:79. The reference drug *Fluconazole* links with multiple hydrogen bond such as THR C:51, PRO H:103, LYS C:48, GLY H:104, PRO C:49, GLY H:107.

Considering these investigations, the synthesized pyrazoline derivatives demonstrated significant antimicrobial potency in the *in vitro*. The computational modeling studies also showed improved binding affinities compared to the standard drugs. These results suggest that the synthesized compounds have the potential to be developed as new effective antimicrobial against bacteria and fungus strain.

Quantum chemical computations

Global chemical reactivity indices for 4,5-dihydro-3-(2,3-dihydrobenzo[b] [1,4] dioxin-7-yl)-1,5-(substituted phenyl)-1*H*-pyrazolines

The global chemical reactivity descriptors were calculated using DFT, this provides valuable insights into the structure-stability-reactivity relationships of the synthesized compounds. Molecular reactivity is determined by the energies of HOMO and LUMO, which are crucial quantum chemical parameters that are used to produce significant descriptors like electron affinity (EA), ionization potential (IP),

Table 8 — HOMO and LUMO orbital energies, HOMO–LUMO gap and Reactivity indexes, electronic chemical potential (μ), chemical hardness (η) and electrophilicity (ω), (all in eV) of 4,5-dihydro-3-(2,3-dihydrobenzo[b] [1,4] dioxin-7-yl)-1,5-(substituted phenyl)-1*H*-pyrazolines.

Entry	E_{HOMO} (eV)	E_{LUMO} (eV)	$\Delta E=E_{LUMO}-E_{HOMO}$ (eV)	Ionization potential (IP)	Electronegativity (χ)	Electronic chemical potential (μ)	Global hardness (η)	Chemical softness (S)	Global electrophilicity index (ω)
1	–5.201	–1.713	3.488	5.201	3.457	–3.457	1.744	0.287	3.427
2	–5.145	–0.884	4.261	5.145	3.015	–3.015	2.131	0.235	2.133
3	–5.113	–1.370	3.743	5.113	3.242	–3.242	1.871	0.267	2.808
4	–5.001	–1.273	3.728	5.001	3.137	–3.137	1.864	0.268	2.640
5	–4.768	–1.057	3.711	4.768	2.912	–2.912	1.856	0.269	2.285
6	–4.952	–1.228	3.724	4.952	3.090	–3.090	1.862	0.269	2.564
7	–7.112	–2.878	4.234	7.112	4.995	–4.995	2.117	0.236	5.892
8	–7.462	–0.884	6.583	7.462	4.176	–4.176	3.291	0.152	2.649
9	–5.067	–2.628	2.440	5.067	3.847	–3.847	1.220	0.410	6.068

absolute electronegativity (χ), chemical potential (μ), softness (σ), hardness (η), and electrophilicity (ω). Among these, high hardness (η) indicates low binding potential whereas high softness (σ) suggests strong binding interactions[42]. Moreover, lower electronegativity (χ) values are generally associated with increased receptor binding affinity. The chemical potential (μ) indicates the ability to donate or accept electrons, where higher values suggest stronger binding interactions.

An examination of the parameters in Table 8, shows that compound **7,** methyl substituent has the highest electronegativity (χ) value of 4.995eV, identifying it as the strongest electron-withdrawing compound in the series. Additionally, pyrazoline **7** exhibits the highest chemical potential (μ) at –4.995eV, suggesting its enhanced ability to accept electrons. Conversely, compound **5**, which has the highest HOMO energy (–4.768eV) and ionization potential (IP) of 4.768eV, is anticipated to easily donate electrons and the smallest value is shown by **8** and **7** which have the most electron-acceptor substituents. In terms of stability, compound **8** exhibits the highest hardness (η) of 3.291 eV among the compounds, indicating it is the most inert, whereas compound **9**, with a hardness of 1.220 eV, is expected to be the most reactive. Moreover, the softness (σ) order of **9 > 1 > 5 > 6 > 4** agrees with this relative reactivity trend. The electrophilicity index- ω, provides information for comparing two molecules, indicating which one acts as an electrophile or nucleophile, with a higher ω value signifying an electrophile and a lower ω value indicating a nucleophile. In this case the highest value of ω was found for compound **9**, which has the most electron-attracting substituent. On the other hand, the smallest value of ω was found for compound **2** which has the most electron-donor substituent.

HOMO and LUMO analysis

There are multiple methods to calculate excitation energies, with the simplest involving the difference between the highest occupied molecular orbital (HOMO) and the lowest unoccupied molecular orbital (LUMO) of the neutral system. Table 9 shows the HOMO and LUMO orbitals of the title compound obtained by B3LYP/6-311G* method. A molecule with a small frontier orbital gap is more polarizable and is generally associated with a high chemical reactivity, low kinetic stability and is also termed as a soft molecule, here compound **9** has less energy gap 2.440(eV), than all other compounds.

Mulliken charge

The bar-diagram of Mulliken charge distribution is portrayed in Fig. 7. Mulliken atomic charge values of pyrazolines are tabulated in the Table 10. From the values of tables, all hydrogen atoms are positive values, hence they are electropositive.

The large negatively charged atoms are present in compound **8** among the other, 14-N charge is –0.8012, 10-O charge is –0.6809 and is shown in Fig. 8. whereas 19-C carbon atom is the most electropositive carbon atom with charge density of 0.43339. Remaining compound's values were highlighted in the Table 10.

MEP study

The molecular electrostatic potential (MEP) maps offer essential insights into the distribution of electron density and electrostatic potential in all pyrazolines,

Table 9 — The HOMO and LUMO orbitals of the synthesised 4,5-dihydro-3-(2,3-dihydrobenzo[b][1,4]dioxin-7-yl)-1,5-(substitutedphenyl)-1*H*-pyrazolines

Entry	HOMO		LUMO
1	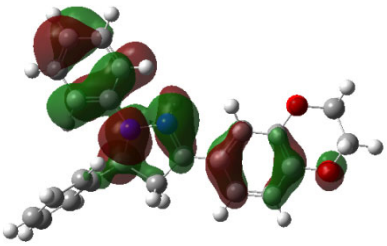	12a △E= 3.488	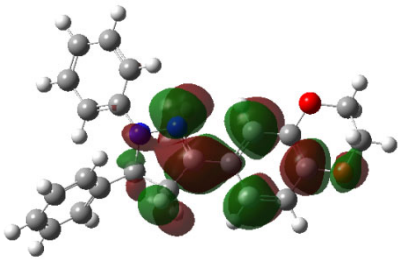
2	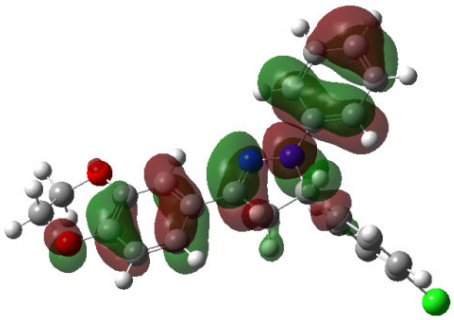	12b △E= 4.621	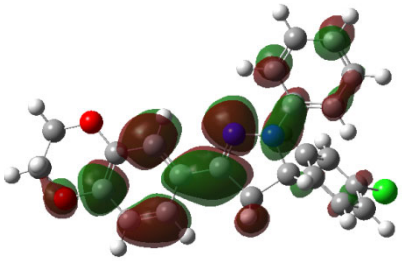
3	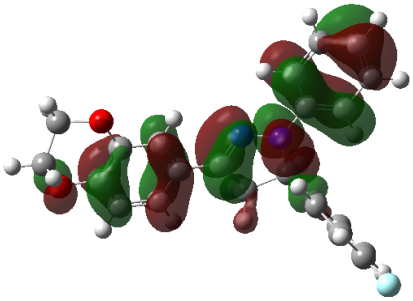	12c △E= 3.743	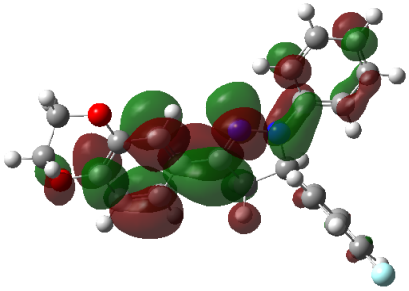
4	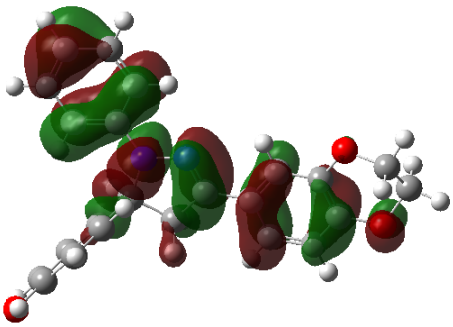	12d △E= 3.728	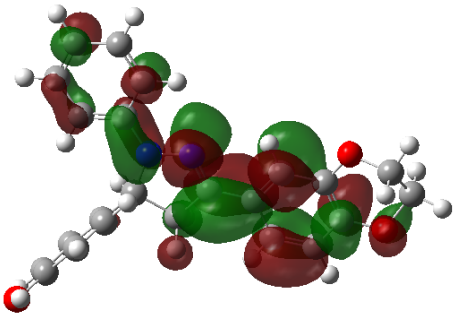
5	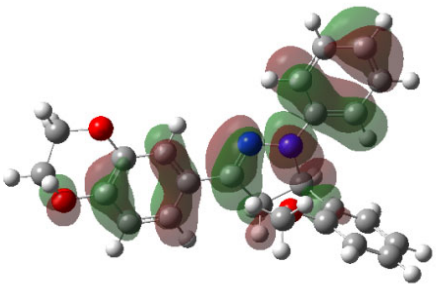	12e △E= 3.711	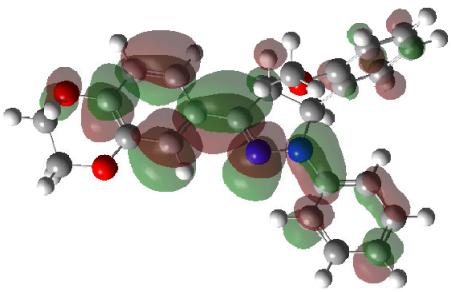

(*Contd.*)

Table 9 — The HOMO and LUMO orbitals of the synthesised 4,5-dihydro-3-(2,3-dihydrobenzo[b][1,4]dioxin-7-yl)-1,5-(substitutedphenyl)-1*H*-pyrazolines (*Contd.*)

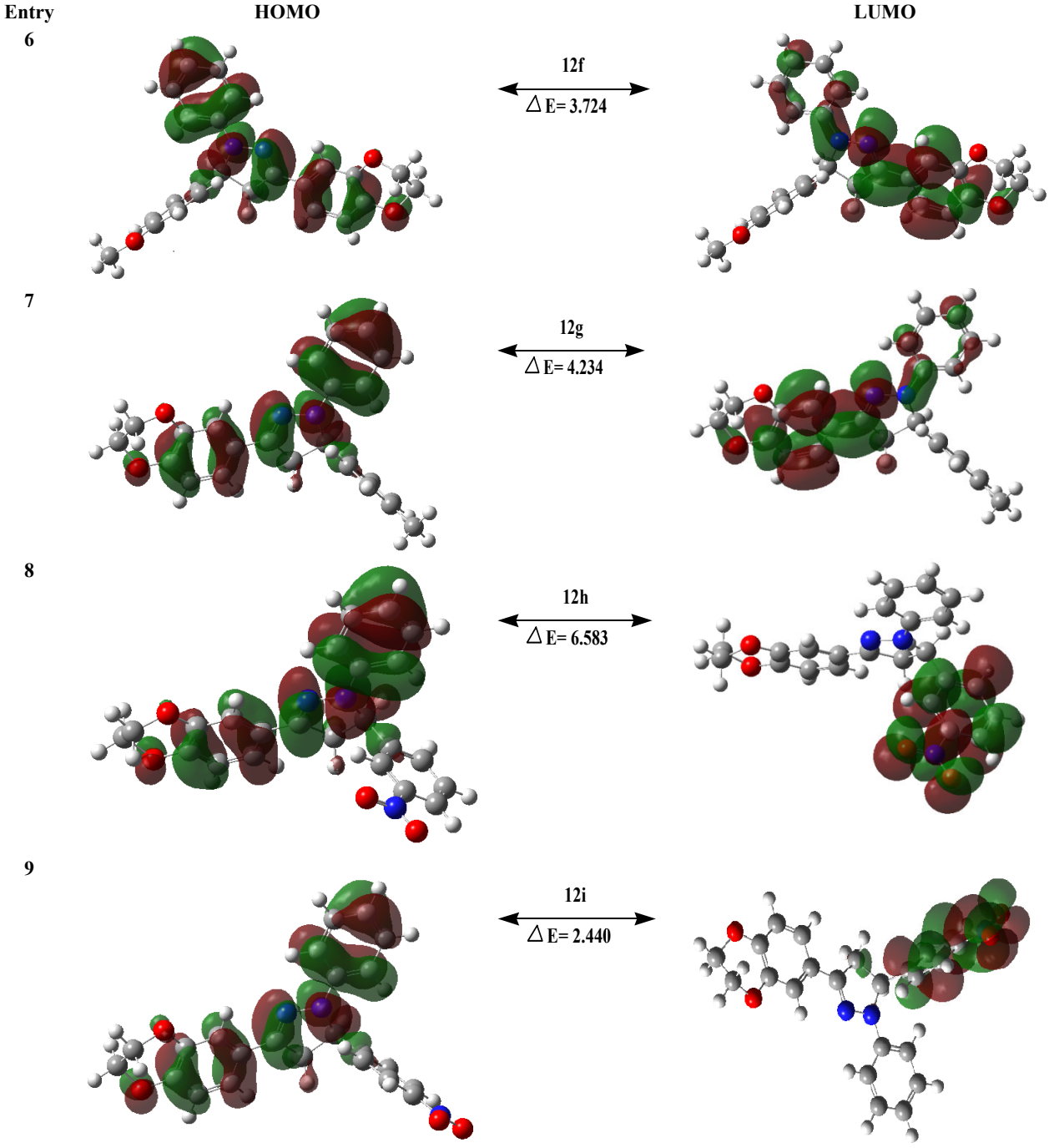

supporting their predicted reactivity. As depicted in Fig. 9, the MEP maps were generated by DFT calculations. In these maps, red regions indicate areas of high electron density that function as nucleophiles, while blue regions denote areas of low electron density corresponding to electropositive sites susceptible to electrophilic addition reactions. For all compounds, the red regions are concentrated on the electronegative (electron rich) heteroatoms (N, O, and S), whereas the blue regions are distributed over the electropositive (electron deficient) phenyl rings. The complementary electrostatic potentials can facilitate

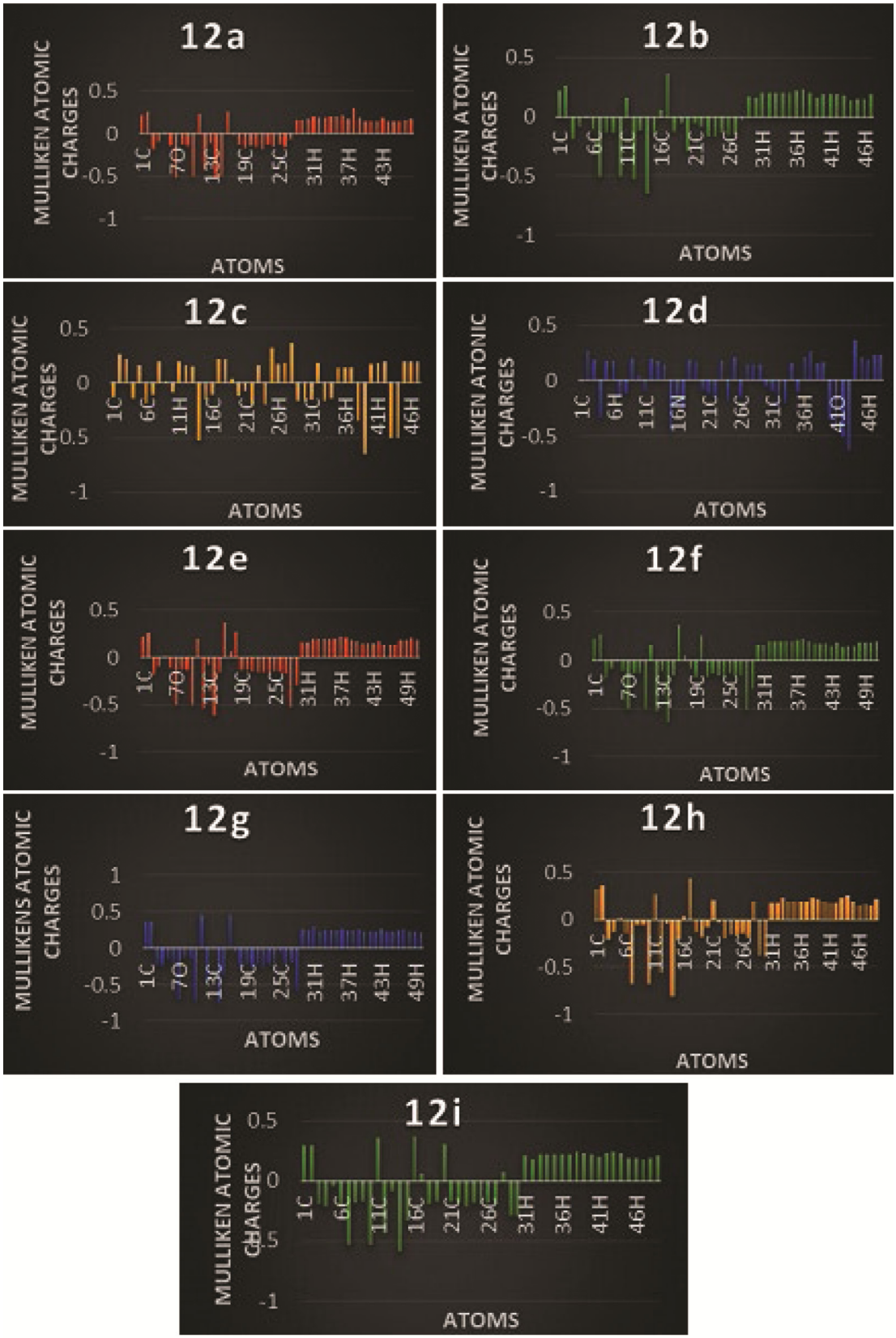

Fig. 7 — The graphical presentation of the Mulliken charge of pyrazolines (**1-9**)

Table 10 — Mulliken atomic charges of the derived pyrazolines

1		2		3		4	
Atom	Charge	Atom	Charge	Atom	Charge	Atom	Charge
1C	0.2180	1C	0.22522	1C	–0.1359	1C	–0.0172
2C	0.2554	2C	0.26581	2C	0.2657	2C	0.26736
3C	–0.1882	3C	–0.1864	3C	0.2250	3C	0.19206
4C	–0.1011	4C	–0.0904	4C	–0.1390	4C	–0.3402
5C	0.0083	5C	0.00929	5H	0.1667	5H	0.17329
6C	–0.144	6C	–0.1048	6C	–0.1866	6H	0.17888
7O	–0.5121	7O	–0.507	7C	–0.1053	7C	–0.1363
8C	–0.133	8C	–0.1398	8H	0.1968	8C	–0.1190
9C	–0.1379	9C	–0.1354	9C	0.0092	9H	0.19756
10O	–0.5097	10O	–0.5081	10C	–0.0903	10C	0.04688
11C	0.2245	11C	0.15463	11H	0.1972	11C	–0.0960
12C	–0.4336	12C	–0.527	12H	0.1577	12H	0.20253
13C	–0.1139	13C	–0.1123	13C	0.1540	13H	0.17352
14N	–0.5045	14N	–0.6476	14C	–0.5274	14C	0.14118
15N	–0.5072	15N	–0.1543	15N	–0.1548	15C	–0.4528
16C	0.2568	16C	0.05249	16C	–0.1108	16N	–0.2489
17C	–0.0039	17C	0.36626	17H	0.2251	17C	–0.2476
18C	–0.1244	18C	–0.1310	18H	0.2166	18H	0.19472
19C	–0.1746	19C	–0.0576	19C	0.0358	19C	0.16736
20C	–0.1387	20C	–0.2895	20C	–0.1148	20C	–0.0871
21C	–0.1577	21C	–0.0537	21C	–0.075	21C	–0.1142
22C	–0.1810	22C	–0.0912	22C	–0.1994	22C	–0.1581
23C	–0.1277	23C	–0.1635	23H	0.1580	23H	0.18276
24C	–0.1644	24C	–0.1677	24C	–0.1958	24C	–0.1856
25C	–0.1277	25C	–0.1384	25C	0.3161	25H	0.21063
26C	–0.1618	26C	–0.1584	26H	0.1798	26C	–0.1470
27C	–0.0775	27C	–0.1605	27H	0.1824	27H	0.15095
28H	0.1614	28Cl	–0.0233	28C	0.3670	28H	0.14947
29H	0.1536	29H	0.16716	29C	–0.1606	29H	0.14335
30H	0.1706	30H	0.15775	30C	–0.1637	30C	–0.0494
31H	0.1974	31H	0.19708	31C	–0.1585	31C	–0.0900
32H	0.1924	32H	0.19716	32H	0.1866	32C	–0.2443
33H	0.1924	33H	0.20141	33C	–0.1679	33C	–0.2068
34H	0.1982	34H	0.20236	34C	–0.1387	34H	0.16093
35H	0.1965	35H	0.19640	35H	0.1436	35C	–0.1016
36H	0.2216	36H	0.21757	36H	0.1420	36H	0.21155
37H	0.1737	37H	0.22569	37H	0.1451	37C	0.26944
38H	0.3080	38H	0.19757	38F	–0.3398	38H	0.15846
39H	0.1906	39H	0.15894	39N	–0.6478	39H	0.17213
40H	0.1437	40H	0.18671	40H	0.1754	40N	–0.3532
41H	0.1463	41H	0.18917	41H	0.1855	41O	–0.4545
42H	0.1451	42H	0.18642	42H	0.1962	42O	–0.5111
43H	0.1860	43H	0.17484	43O	–0.5072	43O	–0.6291
44H	0.1516	44H	0.14265	44O	–0.5082	44H	0.36985
45H	0.1501	45H	0.14555	45H	0.2012	45H	0.21494
46H	0.1521	46H	0.14408	46H	0.1961	46H	0.19323
47H	0.1524	47H	0.18690	47H	0.2022	47H	0.23448
48H	0.1782					48H	0.23345

(Contd.)

Table 10 — Mulliken atomic charges of the derived pyrazolines (*Contd*.)

5		6		7		8		9	
Atom	Charge	Atom	Charge	Atom	Charge	Atom	Charge	Atom	Charge
1C	0.22285	1C	0.2249	1C	0.37052	1C	0.32867	1C	0.29475
2C	0.26299	2C	0.2643	2C	0.37066	2C	0.36760	2C	0.29263
3C	–0.18811	3C	–0.18688	3C	–0.2457	3C	–0.2034	3C	–0.1948
4C	–0.09391	4C	–0.09116	4C	–0.2359	4C	–0.1350	4C	–0.2114
5C	0.00634	5C	0.00951	5C	–0.1462	5C	0.02895	5C	–0.0452
6C	–0.10733	6C	–0.10512	6C	–0.2116	6C	–0.1386	6C	–0.1914
7O	–0.50825	7O	–0.50751	7O	–0.7137	7O	–0.6768	7O	–0.5364
8C	–0.14	8C	–0.1389	8C	–0.1284	8C	–0.0582	8C	–0.1777
9C	–0.13325	9C	–0.13547	9C	–0.1273	9C	–0.0489	9C	–0.1772
10O	–0.51037	10O	–0.50904	10O	–0.7161	10O	–0.6809	10O	–0.5364
11C	0.19142	11C	0.15473	11C	0.44417	11C	0.26507	11C	0.35856
12C	–0.54485	12C	–0.53054	12C	–0.469	12C	–0.5547	12C	–0.441
13C	–0.07057	13C	–0.10853	13C	–0.0021	13C	–0.0433	13C	–0.0880
14N	–0.62199	14N	–0.64383	14N	–0.7806	14N	–0.8012	14N	–0.5885
15N	–0.16344	15N	–0.1576	15N	–0.3709	15N	–0.2059	15N	–0.3317
16C	0.37222	16C	0.36629	16C	0.44499	16C	0.03249	16C	0.36647
17C	0.06500	17C	0.05363	17C	–0.0552	17C	0.43339	17C	0.05721
18C	0.26537	18C	–0.08691	18C	–0.2764	18C	–0.1323	18C	–0.1965
19C	–0.13907	19C	–0.17162	19C	–0.2185	19C	–0.1818	19C	–0.1693
20C	–0.12998	20C	–0.25257	20C	–0.2678	20C	–0.0763	20C	0.30259
21C	–0.14608	21C	–0.1715	21C	–0.2193	21C	0.20462	21C	–0.1679
22C	–0.16653	22C	–0.13603	22C	–0.2656	22C	–0.033	22C	–0.1839
23C	–0.16355	23C	–0.16121	23C	–0.2253	23C	–0.1934	23C	–0.2094
24C	–0.16613	24C	–0.16876	24C	–0.2255	24C	–0.1586	24C	–0.1856
25C	–0.14575	25C	–0.14	25C	–0.0747	25C	–0.1726	25C	–0.1952
26C	–0.15376	26C	–0.15826	26C	–0.2212	26C	–0.1475	26C	–0.1867
27C	–0.17429	27C	–0.16194	27C	–0.2111	27C	–0.1823	27C	–0.1954
28O	–0.53542	28O	–0.52122	28C	–0.5865	28N	0.19782	28N	0.07370
29C	–0.28986	29C	–0.29146	29H	0.26807	29O	–0.3797	29O	–0.2886
30H	0.16350	30H	0.16535	30H	0.24606	30O	–0.3913	30O	–0.2911
31H	0.15651	31H	0.15737	31H	0.29679	31H	0.18613	31H	0.20639
32H	0.19642	32H	0.19673	32H	0.23499	32H	0.17483	32H	0.18293
33H	0.19442	33H	0.19588	33H	0.23921	33H	0.22599	33H	0.22412
34H	0.20001	34H	0.20049	34H	0.23811	34H	0.19541	34H	0.22376
35H	0.19873	35H	0.20135	35H	0.23647	35H	0.19139	35H	0.22302
36H	0.19367	36H	0.19496	36H	0.26309	36H	0.19022	36H	0.22233
37H	0.22731	37H	0.21335	37H	0.24713	37H	0.19453	37H	0.22523
38H	0.20704	38H	0.22481	38H	0.24350	38H	0.23109	38H	0.23824
39H	0.18822	39H	0.19125	39H	0.25373	39H	0.22038	39H	0.23146
40H	0.17148	40H	0.17465	40H	0.23563	40H	0.19449	40H	0.22224
41H	0.15070	41H	0.17132	41H	0.22971	41H	0.17996	41H	0.19765
42H	0.15014	42H	0.16994	42H	0.23604	42H	0.17888	42H	0.2346
43H	0.15127	43H	0.14704	43H	0.26979	43H	0.23476	43H	0.23751
44H	0.17736	44H	0.17851	44H	0.23133	44H	0.26154	44H	0.22633
45H	0.13612	45H	0.13926	45H	0.23417	45H	0.18761	45H	0.18955
46H	0.14099	46H	0.14287	46H	0.23813	46H	0.15609	46H	0.18489
47H	0.13916	47H	0.14177	47H	0.26816	47H	0.16229	47H	0.1797
48H	0.18451	48H	0.18552	48H	0.22393	48H	0.15902	48H	0.18549
49H	0.18791	49H	0.18239	49H	0.22032	49H	0.21326	49H	0.20905
50H	0.21122	50H	0.18109	50H	0.21106				
51H	0.17946	51H	0.20134						

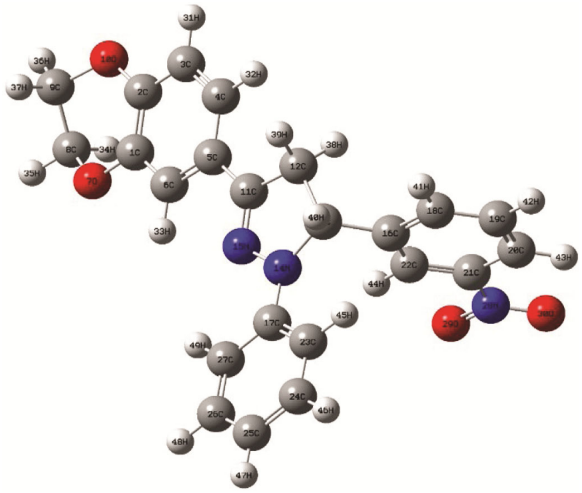

Fig. 8 — Optimized structure with atomic labelling of compound (**8**).

molecular recognition processes like drug receptor binding by enabling attractive interactions between electronegative and electropositive sites.

The MEP is very beneficial tool in the research of correlation between molecular structure and the physiochemical property relationship of molecules containing bio molecules and drugs. According to the current analysis of the MESP plot, the molecule **8** and **9** could experience electrophilic aromatic substitution reactions at the phenyl ring connected to a nitrogen atom because it is highly susceptible to react with electrophilic reagents.

ADME/T analysis

ADME/T analysis was performed to use the molecules as advanced drugs, Drug likeness is a

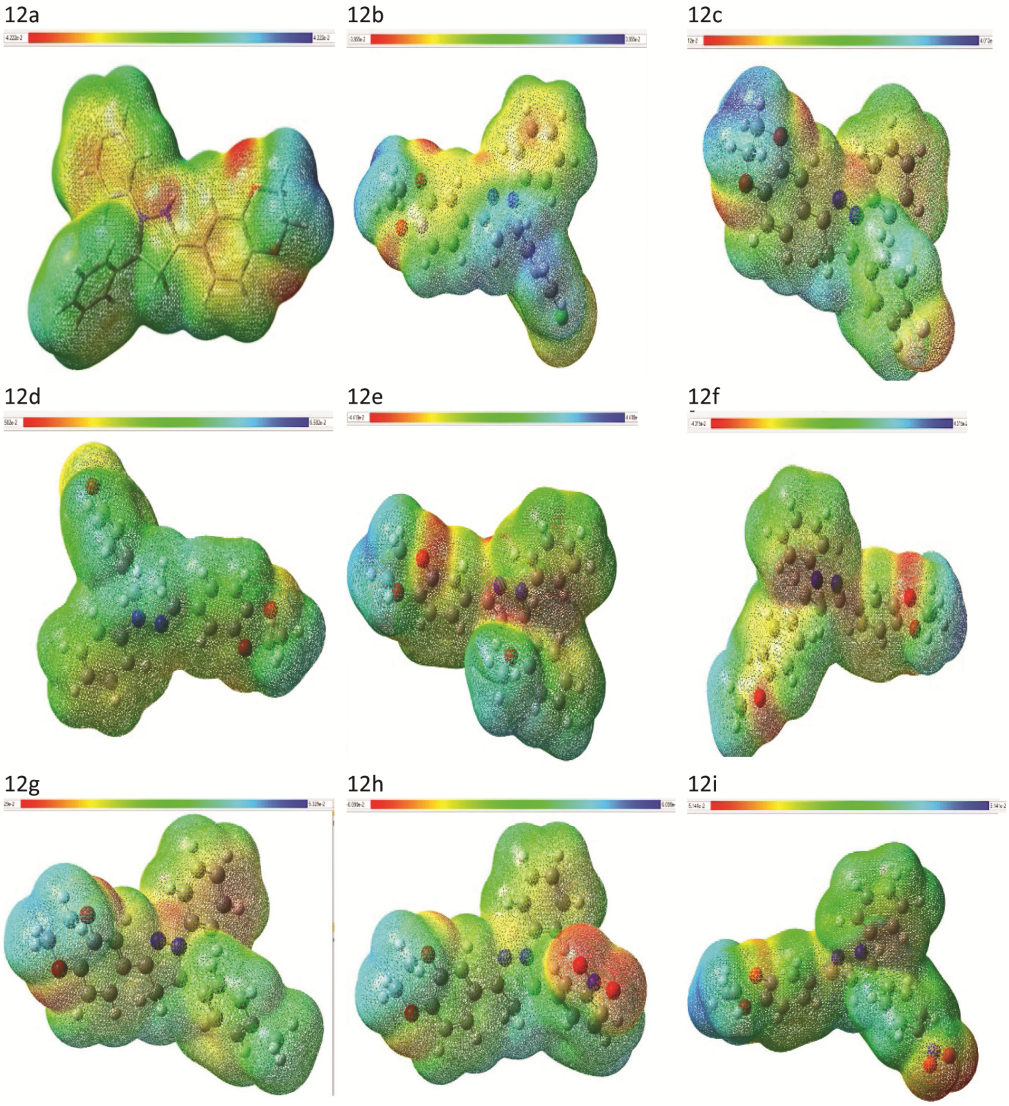

Fig. 9 — Molecular electrostatic potentials (MEP) of compounds (**1-9**)

complex balance of structural features and a molecular property, with this analysis, the behavior of molecules in human metabolism of its pharmacological activity which is similar to drugs is tried to be predicted theoretically. Furthermore, it provides information about how drugs or molecules are absorbed by human tissues and organs and their functions like absorption, distribution, metabolism and excretion (ADME). Among the parameters to be examined for this analysis, the most important parameters are Rule of Five (Lipinski's Rule). These parameters stating that a compound should have a molecular weight less than 500 Da (MW), lipophilicity (Log P), not more than 5 hydrogen bond donors (HBD), not more than 10 hydrogen bond acceptors (HBA), and a calculated log P (Partition coefficient) value less than 5 and TPSA ≤ 140. This is Rule of five. ADME results from the SwissADME program for the compounds are given in Table 11. The pharmacokinetics for the all the compounds has high gastrointestinal (GI) absorption, and blood brain barrier (BBB) permeation. A range of cytochromes (CYP's) regulates the drug metabolism, particularly the biotransformation of drug molecules are regulated by CYP1A2, CYP2C19, CYP2C9, CYP2D6 and CYP3A4[50]. Table 12 displays the pharmacokinetics for the synthesized compounds.

In silico predicted physicochemical and pharmacokinetic properties

From these results, lipophilicity has an important role in shaping many ADME parameters. The distribution of drug molecules between the lipid composition of the cell membrane and the aqueous environment outside of it is measured by the Log P. Compounds characterized by a greater Log P value

Table 11 — ADME prediction values of 4,5-dihydro-3-(2,3-dihydrobenzo[b] [1,4] dioxin-7-yl)-1,5-(substituted phenyl)-1*H*-pyrazolines and standard reference drugs

Entry	n-Heavy atoms	MW	Log P	NHA	NHD	M. Rty	n-violation (Lipinski's Rule of Five)	Log S	TSPA (Å)	% Abs
1	27	356.42	3.37	3	0	113.13	0	–5.19	34.06	97.24
2	28	390.86	4.18	3	0	118.14	1	–5.84	34.06	97.24
3	28	374.41	4.08	4	0	113.09	0	–5.29	34.06	97.24
4	28	372.42	3.14	4	1	115.15	0	–5.24	54.29	90.77
5	29	386.44	3.35	4	0	119.62	0	–5.35	43.29	94.06
6	29	386.44	3.35	4	0	119.62	0	–5.35	43.29	94.06
7	28	370.44	3.91	3	0	118.1	0	–5.56	34.06	97.24
8	30	401.41	3.55	5	0	121.95	0	–5.97	79.88	81.64
9	30	401.41	3.55	5	0	121.95	0	–5.97	79.88	81.64
Chlo	20	323.13	1.14	5	3	74.38	0	–2.71	115.3	90.84
Flu	22	306.27	1.47	5	1	70.71	0	–1.63	81.65	90.50

NHD-number of hydrogen donor; NHA-number of hydrogen acceptor; NRB-number of rotatable bonds; TPSA- total polar surface area; Abs- absorption, Chlo- Chloramphenicol; Flu- Fluconazole

Table 12 — Predicted pharmacokinetics for the synthesized compounds 4,5-dihydro-3-(2,3-dihydrobenzo[b] [1,4] dioxin-7-yl)-1,5- -(substituted phenyl)-1*H*-pyrazolines and standard reference drugs

Entry	GI absorption	BBB permeation	Kp-Skin permeation (cm/s)	CYP1 A2 inhibitor	CYP2C 19 inhibitor	CYP2 C9 inhibitor	CYP2 D6	CYP3 A4	P-gp substrate	Bioavailability score
1	High	Yes	–5.11	Yes	Yes	Yes	Yes	Yes	Yes	0.55
2	High	Yes	–5.21	Yes	Yes	Yes	No	Yes	Yes	0.55
3	High	Yes	–5.11	Yes	Yes	Yes	Yes	Yes	Yes	0.55
4	High	Yes	–5.46	Yes	Yes	Yes	Yes	Yes	Yes	0.55
5	High	Yes	–5.31	Yes	Yes	Yes	Yes	Yes	Yes	0.55
6	High	Yes	–5.31	Yes	Yes	Yes	Yes	Yes	Yes	0.55
7	High	Yes	–4.94	Yes	Yes	Yes	Yes	Yes	Yes	0.55
8	High	No	–5.50	Yes	Yes	Yes	No	Yes	No	0.55
9	High	No	–5.50	Yes	Yes	Yes	No	Yes	No	0.55
Chlo	High	No	–7.46	No	No	No	No	No	No	0.55
Flu	High	No	–7.92	No	Yes	No	No	No	Yes	0.55

Chlo- Chloramphenicol; Flu- Fluconazole.

exhibit reduced polarity and inferior solubility in water[51]. All the compounds ranged from (3.14 to 4.18) have good ADME properties in the lipid region and reference drugs are 1.14 &1.47. The predicted water solubilities Log S indicate that all compounds are more soluble in aqueous environments.

The pharmacokinetic properties of the studied compounds in Table 12, implies that Kp values of all molecules are within the range of (–5.11to –5.50 cm/s) with chloramphenicol (–7.21cm/s) and fluconazole (–7.92cm/s) inferring low skin permeability. All the compounds have high gastrointestinal (GI) absorption, this score indicates rapid digestion and absorption of synthesized compounds in the small intestine and blood brain barrier (BBB) permeation. Blood-brain barrier permeability, which is demonstrated by compounds **1** to **7** but not by compounds **1** and **9**. These findings suggest that compounds **1** to**7** can penetrate the central nervous system (CNS), which is shown in Fig. 10. Boiled egg prediction of all compounds explains that compounds penetrate inside the yellow yoke of boiled egg predictions. Permeability glycoprotein (P-gp) acts as a xenobiotic barrier to the central nervous system. The synthesized compounds are effective P-gp substrates and xenobiotic inhibitors except compounds **8** and **9**. Finally, Bioavailability score for all the compound is 0.55 which is lesser than value 1.

Toxicity

The smile notations extracted from Swiss ADME were inserted on the interface of Osiris property explore. It obtains active and inactive descriptors of the examined compounds, reflecting their toxicity assessment the color-coded toxicity results for valid chemical structures. The synthesized pyrazoline analogs exhibit green/safe(inactive) indications for mutagenic and irritant features, while the explorer predicts high toxicity/red alerts(active) for Organ Toxicity, as listed in Table 13.

Though computational studies offered valuable insights, they did not entirely predict the potency of certain pyrazolines, which was subsequently verified through experimental findings. This discrepancy highlights the complementary connection between computational and empirical methodologies in the process of drug discovery. Our research not only advances the growing corpus of knowledge in the area of antimicrobial drug development but also facilitates the further refinement of pyrazoline-based compounds.

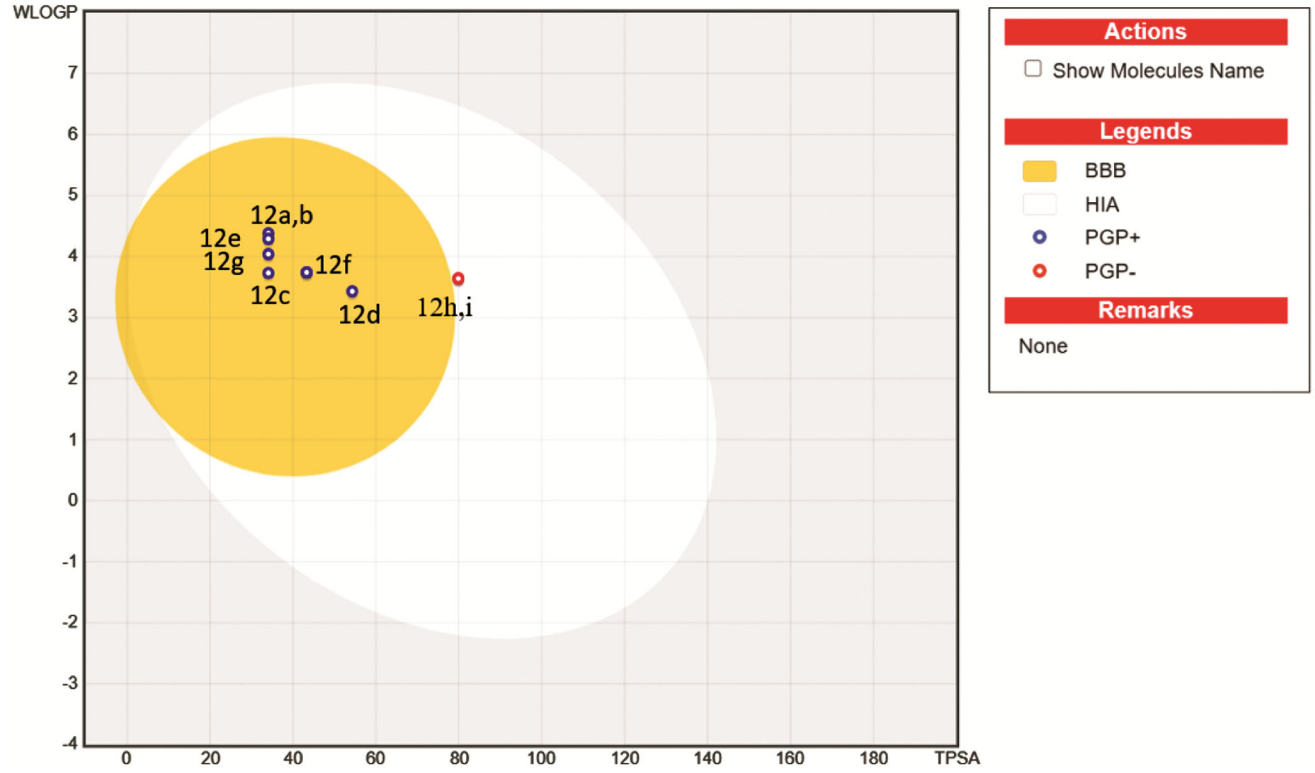

Fig. 10 — Boiled egg prediction of synthesised pyrazolines

Experimental Section

Materials and methods

All of the chemicals were purchased from E-Merck and Sigma-Aldrich. The Mettler FP51 melting point equipment was used to determine the melting temperatures of all pyrazolines in open glass capillaries. IR spectra were recorded on a BRUKER (Thermo Nicolet) Fourier transform spectrophotometer (KBr, 4000–400 cm^{-1}). The NMR spectra of all pyrazolines were acquired using a JEOL-400 spectrometer at 400 MHz for ^{1}H spectra and 100 MHz for ^{13}C spectra in $CDCl_3$ solvent using TMS as an internal standard. The synthesized compound's purity was tested by Silica-TLC Alu foils plates and spots were visualized by using a UV lamp.

General procedure for the synthesis of 4,5-dihydro-3-(2,3-dihydrobenzo[b][1,4]dioxin-7-yl)-1,5-(substitutedphenyl)-1*H*-pyrazolines (1-9).

An equal molar quantity of (*E*)-1-(2,3-dihydrobenzo[b][1,4]dioxin-6-yl)-3-phenylprop-2-en-1-ones[31], phenyl hydrazine hydrochloride, sodium acetate and 20 mL of ethanol were refluxed for 6h (Scheme 2). The contents were cooled before being poured into cold water and stirred slowly. After 10-15 minutes, the precipitate was filtered using a Buckner funnel and dried off. Then it is recrystallized from ethanol by slow evaporation process. The analytical, physical constants of the synthesised (**1-9**) compounds were presented in Table 14.

Antimicrobial potential evaluation

The antibacterial activity of synthesised pyrazolines[22, 25, 32-37] was assessed using common medications as controls, such as fluconazole for fungus and chloramphenicol for bacteria. The test was conducted against four microbial species; *Staphylococcus aureus; Streptococcus pneumonia; Pseudomonas aeruginosa; Escherichia coli* using 15 µL concentration. As a result, in Table 5, the synthesized 4,5-dihydro-3-(2,3-dihydrobenzo[b] [1,4] dioxin-7-yl)-1,5-(substituted phenyl)-1*H*-pyrazolines

Table 13 — Predication of toxicity of synthesized 4,5-dihydro-3-(2,3-dihydrobenzo[b][1,4] dioxin-7-yl)-1,5-(substituted phenyl)-1*H*-pyrazolines computed by Osiris property explorer

Entry	Toxicity Class	Organ Toxicity				
		Hepatotoxicity	Carcinogenicity	Cytotoxicity	Mutagenicity	Reproductive Effective
1	4					
2	4					
3	4					
4	4					
5	4					
6	4					
7	4					
8	4					
9	4					
Chl	4					
Flu	4					

Chl: Chloramphenicol; Flu: Fluconazole

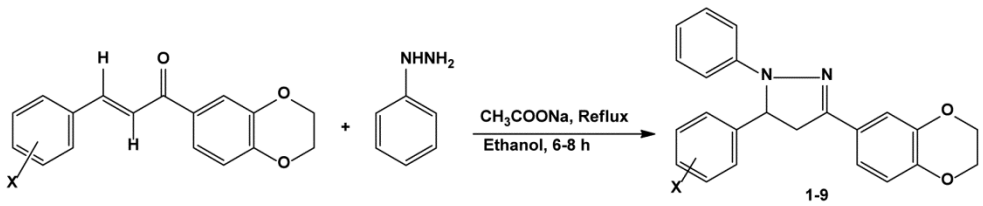

Entry	**1**	**2**	**3**	**4**	**5**	**6**	**7**	**8**	**9**
X	H	4-Cl	4-F	4-OH	3-OCH_3	4- OCH_3	4-CH_3	3-NO_2	4-NO_2

Scheme 2 — Synthesis of 4,5-dihydro-3-(2,3-dihydrobenzo[b][1,4]dioxin-7-yl)-1,5-(substitutedphenyl)-1*H*-pyrazolines

Table 14 — The physiochemical constants, and yield of synthesized 4,5-dihydro-3-(2,3-dihydrobenzo[b][1,4]dioxin-7-yl)-1,5-(substitutedphenyl)-1*H*-pyrazolines

Entry	X	M.F.	M.W	Time (h)	Yield (%)	M.P. (°C)
1	H	$C_{23}H_{20}N_2O_2$	357	6	87	137-138(135-137)[24]
2	4-Cl	$C_{23}H_{19}ClN_2O_2$	391	6.5	92	117-119(116-118)[24]
3	4-F	$C_{23}H_{19}FN_2O_2$	375	7	95	75-77(76-77) [24]
4	4-OH	$C_{23}H_{20}N_2O_3$	372	6.5	80	180-181
5	3-OCH_3	$C_{23}H_{22}N_2O_3$	387	6	83	127-128(125-127)[24]
6	4-OCH_3	$C_{23}H_{22}N_2O_3$	387	6	80	114-115(112-114)[24]
7	4-CH_3	$C_{24}H_{22}N_2O_2$	358	6	88	135-137(134-136)[24]
8	3-NO_2	$C_{23}H_{19}N_3O_4$	401	8	90	127-129
9	4-NO_2	$C_{23}H_{19}N_3O_4$	401	8	85	149-151

were showed good zone of inhibition when compared with the standard drug chloramphenicol. The anti-fungal activity of the synthesized pyrazoline were against *C. albicans* and *C. auris* microbes with standard procedure.

Molecular docking analysis

An essential computational method for drug discovery, molecular docking uses algorithms to forecast the binding affinity and interactions between ligands and target proteins[41]**.** The target proteins were downloaded from the Protein Data Bank, and molecular docking was conducted using Autodock4, MGL tools 1.5.7, Discovery Studio was used to view and evaluate the generated poses for hydrophobicity, electrostatic interactions, and secondary structure. Lastly, each stance was examined in the Discovery studio visualization window, with rendering parameters for colours and styles adjusted. The investigation of hydrophobicity, electrostatic interactions, and secondary structure was made possible by the 3D visualization. In structural molecular biology and computer-assisted drug creation, molecular docking is a crucial application. Docking is employed to perform virtual screening of compound libraries, analyse the results, and propose structural hypotheses regarding how the compounds inhibit the target, which is valuable in lead optimization.[34, 37-41]

Docking studies experimental protocol

The binding affinity analysis of compounds that showed the best inhibitory values in the *in vitro* studies compared to *Chloramphenicol, Fluconazole.* To investigate the probable binding modes and mechanisms of these synthesized compounds, along with the molecular interactions by which these compounds interact with the 7S54 (chimeric sortase A enzyme from the bacteria *Streptococcus aureus*), 9R2Z (RptR transcriptional repressor protein from *Escherichia coli*), 5HW8 (FKBP12 protein from the fungus *Candida albicans*) receptors, computational screening studies were performed. Table 6, lists the binding energies of the discussed compounds with 7S54, 9R2Z, 5HW8 receptors. The molecular docking investigations with the *in-vitro* antimicrobial studies' potent compounds showed significantly good and improved binding affinities with the *Streptococcus aureus* receptor 7S54 of the target receptor compared to the *Chloramphenicol* compound[34,37-41].

Quantum chemical calculations

Gaussian 09 software suite employed for all quantum mechanical calculations. These calculations were carried out using the widely recognized B3LYP functional, known for its accuracy in predicting molecular properties[37, 39, 42-46]. To guarantee reliable results, a 6-311G(d,p) basis set was used. This computational setup was utilized to clarify the electronic structure and reactivity profiles of the synthesized compounds.

Mulliken charge analysis

Mulliken atomic charges are derived from Mulliken population analysis[44]. Partial atomic charges, computational simulations and Mulliken charges being derived from the charge density using B3LYP method with 6-311G* (d,p) set[47].

ADMET evaluation

The drug-likeness and ADMET properties[38, 40, 41, 48] of the title compounds were examined utilizing SwissADME program and discussed for the above synthesized compounds. The Protox Program was used for finding the Toxicity of the synthesized pyrazolines.[37, 48]

Conclusions

In summary, totally nine 4,5-dihydro-3-(2,3-dihydrobenzo[b][1,4]dioxin-7-yl)-1,5-(substitutedphenyl)-1*H*-pyrazolines were synthesized from chalcones. The synthesized compounds structures are confirmed by FT-IR, NMR spectral studies. Further, these compound's chemical shifts and assigned spectrum (IR,^{1}H and ^{13}C NMR) frequencies were associated with the Hammett substituent constants F and R parameters. Regression analysis with its spectrum frequencies reveals satisfied correlations with the help of single and multi-linear regression. The synthesized compounds displayed potent activity against the bacterial and fungal strains. Among them, compound **1** showed maximum activity against *Staphylococcus aureus* and *Escherichia coli* with relative to the standard drug. On the other hand, compound **8** exhibited maximum activity against *Pseudomonas aeruginosa* with relative to the standard drug. In fungal strains the compound **1** showed maximum activity against *Candida auris* with relative to the standard drug. The molecular docking study of the antimicrobial potent compounds was conducted to investigate their binding pattern with *Streptococcus aureus*- 7S54, *Escherichia coli*- 9R2Z, *Candida albicans*- 5HW8 receptors. The computational modeling studies also showed improved binding affinities compared to the standard drugs. DFT analysis of the compounds revealed the presence of electrophilic and nucleophilic bioactive sites of the receptors. The HOMO and LUMO molecular orbitals, along with other quantum parameters, were calculated. The total atomic charge values were calculated using Mulliken population analysis. MEP's were calculated in the optimized geometries. *In silico* evaluations confirmed favorable drug-likeness and pharmacokinetic properties for all analogues, ADMET properties further demonstrated that these compounds possess a good therapeutic application in combating bacterial and fungal infections.

Supplementary Information

Supplementary information is available in the website https://nopr.niscpr.res.in/handle/123456789/58776

References

1 Ju Y & Varma R S, *J Org Chem*, 71 (2006) 135.
2 Manikanta P, Mounesh, Nikam R R, Sandeep S & Nagaraja B M, *J Mat Chem B,* 11 (2023) 1160.
3 Bodke B M, Mounesh Y D & Bhat SA, *RSC Sust,* 2 (2024) 475.
4 Fatima A, Aslam S, Janiad S, Faisal S, Irfan A & Iqbal J, Shazly G A, Zafar M A, Shaheen A, Noreen S, Mateev E & Jardan Y A B, *Mol Divers,* 29 (2025) 5773.
5 Nitulescu G M, Stancov G, Seremet O C, Nitulescu G, Mihai D P & Duta-Bratu C G, Barbuceanu S F & Olaru O T, *Molecules,* 28 (2023) 5359.
6 Raauf A M R, Omar T N A, Mahdi M F & Fadhil H R, *Nat Prod Res,* 38 (2024) 253.
7 Abdel-Aziz A A M, El-Azab A S, Brogi S, Ayyad R R, Alkahtani H M, Abuelizz H A, Al-Suwaidan I A & Al-Obaid A M, *RSC Adv*, 14 (2024) 22132.
8 Ahmed M H, El-Hashash M A, Marzouk M I & El-Naggar A M, *J Hetero Chem,* 56 (2019) 114.
9 Venkatraman R, Divya J, Gayathri P, Thirunarayanan G & Muthuvel I, *Ovidius Univ Annals Chem*, 35 (2024) 36.
10 Shinde R A, Adole V A & Jagdale B S, *Poly Arom Comp,* 42 (2022) 6155.
11 Ugras Z, Tok F, Çakir C, Tuna K, Tatar-Yilmaz G, Mutlu D, Sicak Y, Arslan S, Ozturk M & Kocyigit-Kaymakcioglu B, *J Mol Struc*, 1315 (2024) 138978.
12 Ang W, Chen G, Xiong L, Chang Y, Pi W, Liu Y, Li C, Zheng J, Zhou L, Yang B, Deng Y, Yang S, Luo Y & Wei Y, *Euro J Med Chem*, 82 (2014) 263.
13 Ochi T, Jobo-Magari K, Yonezawa A, Matsumori K & Fujii T, Euro. *J Pharm,* 365 (1999) 259.
14 Vashisht K, Sethi P, Mishra P & Bansal A, *Res J Chem Environ*, 26 (2022)184.
15 Secci D, Bolasco A, Chimenti P & Carradori S, *Curr Med Chem*, 18 (2011) 5114.
16 Duan L M, Yu H Y, Li Y L & Jia C J, *Bioorg Med Chem*, 23(2015) 6111.
17 Martins D M, Torres B G, Spohr P R, Machado P, Bonacorso H G, Zanatta N, Martins M A & Emanuelli T, *Basic Clin Pharm Tox,* 104 (2009) 107.
18 Kenchappa R, Bodke Y D, Chandrashekar A, Aruna Sindhe M & Peethambar S K, *Arab J Chem,* 10 (2017) 3895.
19 Rehse K, Kotthaus J & Khadembashi L, *Archiv Der Pharm*, 342 (2009) 27.
20 Ravula P, Vamaraju H B, Paturi M, Chandra J N N S & Kolli S, *Excel J*, 15 (2016) 187.
21 Nehra B, Rulhania S, Jaswal S, Kumar B, Singh G & Monga V, *Eur J Med Chem*, 205 (2020) 112666.
22 Sakthinathan S P, Vanangamudi G & Thirunarayanan G, *Spectrochim Acta Part A: Mol Biomol Spect*, 95 (2012) 693.
23 Thirunarayanan G, Mayavel P, Thirumurthy K, Dineshkumar S, Sasikala R, Nisha P & Nithyaranjani P, *Eur Chem Bull*, 2 (2013) 598.
24 Yang YS, Yang B, Zou Y, Li G & Zhu H L, *Bio Med Chem*, 13 (2016) 3052.
25 Sasikala S, Thirumurthy K, Mayavel P & Thirunarayanan G, *Org Med Chem Lett*, 2 (2012) Article No. 20. (https://doi.org/10.1186/2191-2858-2-20).
26 Thirunarayanan G & Sekar K G, *World Res J Org Chem*, 2(2014) 15.
27 Thirunarayanan G & Sekar K G, *Org Chem: An Indian J*, 10(2014) 43.
28 Thirunarayanan G & Sekar K G, *J Taibah Univ Sci,* 8 (2014) 124.
29 Thirunarayanan G & Sekar K G, *Modern Org Chem Res*, 2 (2017) 139.

30 Swain C G & Lupton E C, *J Am Chem Soc*, 90 (1968) 4328.
31 Srinivasan S & Thirumalmurugan S, *Chem Sci Rev Lett,* 24(2017) 2506.
32 Bauer A W, Kirby W M M, Sherris J C & Truck M, *Am J Clin Path*, 45 (1996) 493.
33 Thirunarayanan G, Dineshkumar N & Rajarajan M, *World Scientific News*, 117 (2019) 14.
34 Gayathri P, Divya J, Muthuvel I, Usha V, Malar Retna & Thirunarayanan G, *Indian J Chem*, 64 (2025) 670.
35 Gayathri P, Muthuvel I, Mayavel P, Ranganathan K, Usha V, Mala V & Thirunarayanan G, *Ovidius Univ Annal Chem*, 36 (2025) 66.
36 Gayathri P, Divya J, Muthuvel I, Mayavel P, Usha V, Nalini S, Manikandan V, Sundararajan R, Arulkumaran R, Sakthinathan S P & Thirunarayanan G, *Ovidius Univ Annal Chem*, 35 (2025) 146.
37 Gayathri P, Mayavel P, S. Balasundari, P Sudha, Muthuvel I, Usha, Ranganathan K, Krishnakumar B, Rajasree S, Veeravelan K & Thirunarayanan G, *Indian J Chem*, 65 (2026) 145.
38 Muthuvel I, Divya J, Gayathri P, Balasundari S, Sudha P, Palanivel, Krishnakumar B, Manikanadan V, Alanazi A K & Thirunarayanan G, *Indian J Chem*, 64 (2025) 94.
39 Venkatraman R, Divya J, Gayathri P, Muthuvel I & Thirunarayanan G, *Indian J Chem*, 64 (2025) 465.
40 Dinesh kumar N, Thirunarayanan G, Elancheran R, Suppuraj P, Guganathan L, Sivasakthikumar R, Ramkuma S & Swaminathan M, *J Mol Struc*, 1322 (2025) 140603.
41 Divya J, Gayathri P, Muthuvel I, Suguna S & Thirunaryanan G, *Chem Sel*, 9 (2025) e202402276.
42 Alshaye N A, Alharbi N S, El-Atawy M A, Omar A Z, Hamed E A, Elhag M, Ahmed H A & El-Zawawy R O, *Heliyon*, 10 (2024) 14.
43 Faundez-Gutierrez R, Macleod-Carey D, Zarate X, Bustos C, Molins E & Schott E, *Polyhedron*, 81 (2014) 414.
44 Dineshkumar N, Suppuraj P, Mayavel P, Muthuvel I & Thirunarayanan G, *Mat Today Proc*, 29 (2020) 1059.
45 Dinesh kumar N, Mayavel P, Muthuvel I & Thirunarayanan G, *Chem Data Coll*, 30 (2020) 100547.
46 Rezan H H S, Aso H H, Awaz j H, Mohammad R S, Sonam S, Joazaizulfazli J, Farouq E H & Mohammad R F P, *Res Chem Int*, 48 (2022) 4729.
47 Mulliken R S, *J Chem Phy,* 23 (1955) 10.
48 Alawad K M, Mahdi M F & Raauf A M R, *J Hunan Univ,* 48 (2021) 9.
49 Rasgania J, Gavadia R, Varma-Basil M, Chauhan V, Kumar S & Mor S, Singh D & Jakhar K, *J Mol Struc*, 1295 (2024) 136657.